Endosomal dysfunction contributes to cerebellar deficits in spinocerebellar ataxia type 6

Anna A. Cook[1], Tsz Chui Sophia Leung[1], Max Rice[1,2], Maya Nachman[1], Élyse Zadigue-Dubé[1], Alanna J. Watt[1*]

[1]Biology Department, McGill University, Montreal, QC, Canada.

[2]Department of Biological Sciences, Columbia University, New York, NY, USA.

[*]Correspondence: alanna.watt@mcgill.ca

Abstract

Spinocerebellar ataxia type 6 (SCA6) is a rare disease that is characterized by cerebellar dysfunction. Patients have progressive motor coordination impairment, and postmortem brain tissue reveals degeneration of cerebellar Purkinje cells and a reduced level of cerebellar brain-derived neurotrophic factor (BDNF). However, the pathophysiological changes underlying SCA6 are not fully understood. We carried out RNA sequencing of cerebellar vermis tissue in a mouse model of SCA6, which revealed widespread dysregulation of genes associated with the endo-lysosomal system. Since disruption to endosomes or lysosomes could contribute to cellular deficits, we examined the endo-lysosomal system in SCA6. We identified alterations in multiple endosomal compartments in the Purkinje cells of SCA6 mice. Early endosomes were enlarged, while the size of the late endosome compartment was reduced. We also found evidence for impaired trafficking of cargo to the lysosomes. As the proper functioning of the endo-lysosomal system is crucial for the sorting and trafficking of signaling molecules, we wondered whether these changes could contribute to previously identified deficits in signaling by BDNF and its receptor tropomyosin kinase B (TrkB) in SCA6. Indeed, we found that the enlarged early endosomes in SCA6 mice accumulated both BDNF and TrkB. Furthermore, TrkB recycling to the cell membrane in recycling endosomes was reduced, and the late endosome transport of BDNF for degradation was impaired. Therefore, mis-trafficking due to aberrant endo-lysosomal transport and function could contribute to SCA6 pathophysiology through alterations to BDNF-TrkB signaling, as well as mishandling of other signaling molecules. Deficits in early endosomes and BDNF localization were rescued by chronic administration of a TrkB agonist, 7,8-DHF, that we have previously shown restores motor coordination and cerebellar TrkB expression. The endo-lysosomal system is thus both a novel locus of pathophysiology in SCA6, and a promising therapeutic target.

Introduction

Spinocerebellar ataxia type 6 (SCA6) is an inherited ataxia which presently has no cure (Solodkin and Gomez, 2012). It is caused by a CAG expansion mutation that generates an expanded polyglutamine tract in the translated protein (Zhuchenko et al., 1997). The affected gene is *CACNA1A* (Zhuchenko et al., 1997), which encodes both the alpha subunit of voltage-gated calcium P/Q channels, as well as a putative transcription factor (Du et al., 2019, 2013). The cellular dysfunction giving rise to disease in SCA6 is poorly understood. Here we examine the role of the endo-lysosomal system in SCA6 pathophysiology.

The endo-lysosomal system comprises of a series of membrane-bound compartments that sort and transport endocytosed molecules destined for recycling or degradation (Fig. 1a) (Hu et al., 2015; Huotari and Helenius, 2011). These compartments are highly dynamic and regularly interact and fuse with each other as cargo is sorted and trafficked. Each compartment has a characteristic pH mediated by ATP-dependent acidification (Hu et al., 2015), and is characterized by the presence of specific proteins that allow them to carry out their functions. Rab GTPases regulate trafficking of cargo, and each compartment is associated with a specific signature of Rab family members (Stenmark, 2009). Endocytosed cargo arrives first at the early endosomes (Ludwig et al., 1991), where the slightly acidic pH leads to dissociation of ligands from their receptors. Here the cargo will undergo sorting: those that are destined for recycling such as receptors, will be returned to the cell surface. Cargo that is destined for further sorting or degradation will move to the late endosomes, which are characterized by an increasingly acidic pH and increased enzymatic activity (Hu et al., 2015; Huotari and Helenius, 2011). The lysosome is the final destination of cargo that is to be degraded. This compartment is the most acidic and contains over 50 hydrolases that carry out rapid degradation of cargo (de Duve, 2005; Lawrence and Zoncu, 2019).

Endosome dysfunction plays a role in the pathophysiology of several neurological diseases. A notable example is Alzheimer's disease, where postmortem brain tissue from patients displays increased early endosome size and accumulation of cargo (Cataldo et al., 2004, 2000, 1997; Tate and Mathews, 2006). Similar early endosome changes are seen in Down syndrome (Cataldo et al., 2000) and Niemann Pick C (Jin et al., 2004; Kim et al., 2023). In the cerebellum, endo-lysosomal dysfunction can lead to cerebellar dysfunction (Akizu et al., 2015; Mannan et al., 2004; Sterling et al., 2023; Vanier, 2010), and has been identified in cerebellar diseases with diverse disease-causing mechanisms (Alves et al., 2014; Zhu et al., 2022). As endosomes are the site of disassociation of ligands from their receptors, mediating both the recycling of receptors back to the cell surface and the sorting of ligands for further signaling or degradation, dysfunction can disrupt signaling pathways due to mis-trafficking of signaling molecules.

Previously, lysosomal accumulation of protein aggregates has been observed in a mouse model of SCA6 (118Q) that features a hyperexpanded polyglutamine repeat (Unno et al., 2012). This suggests that lysosomes may play a role in SCA6. Cerebellar pathology in this model was worsened when lysosomal function was impaired by the loss of the lysosomal enzyme cathepsin B (Unno et al., 2012). However, it has been unknown whether endo-lysosomal pathway dysregulation is implicated in the natural disease progression of SCA6, or whether other endosomal compartments may be involved.

We have recently found that deficits in the BDNF-TrkB-Akt signaling pathway contribute to SCA6 pathophysiology (Cook et al., 2022), with both BDNF and TrkB expression reduced in the cerebellar vermis. However, the underlying causes of the reduced levels of BDNF and TrkB remained unknown. Since both BDNF and TrkB are dynamically trafficked through the endo-lysosomal system (Moya-Alvarado et al., 2023, 2018; Yamashita and Kuruvilla, 2016), we wondered whether dysfunction in this system could underlie BDNF and/or TrkB mislocalization, contributing to subsequent cellular dysfunction in SCA6.

To address whether alterations in the endo-lysosomal system give rise to cellular dysfunction in SCA6, we examined endo-lysosomal compartments in the cerebellum of male and female $SCA6^{84Q/84Q}$ mice (referred to as SCA6 mice) in the early stages of SCA6 progression. In addition to observing abnormalities in endosomal compartments, we found that BDNF and its receptor TrkB accumulated in early endosomes instead of undergoing normal sorting and recycling. These abnormalities were present in SCA6 mice between 7 and 12 months of age, coincident with the onset of motor impairment and long before Purkinje cell degeneration (Jayabal et al., 2015). These changes therefore represent an early driver of SCA6 pathology. We were able to rescue the deficits in early endosomes with chronic administration of the TrkB agonist 7,8-DHF, a treatment that we previously found could also rescue behavioural and Purkinje cell firing deficits in the SCA6 mice. Our findings argue that endo-lysosomal dysfunction is a novel locus of pathophysiology in spinocerebellar ataxia and a potential therapeutic target to investigate further.

Results

The endo-lysosomal system (Fig. 1a) is critical for proper cellular function and its dysregulation is associated with mis-trafficking of important cargo. Here we address whether endo-lysosomal dysfunction contributes to SCA6, using a mouse model ($SCA6^{84Q/84Q}$ mice, referred to as SCA6 mice) that robustly models the mid-life onset of motor deficits and cerebellar dysfunction seen in SCA6 patients (Jayabal et al., 2015; Watase et al., 2008). We have previously shown that around 7 months of age, SCA6 mice develop deficits in motor coordination that progressively worsen (Jayabal et al., 2015, 2016) and display cellular deficits, including aberrant Purkinje cell firing and disrupted BDNF-TrkB signaling (Chang et al., 2022; Jayabal et al., 2016). The cellular alterations that lead to the reduction of BDNF and TrkB in the SCA6 cerebellum remained unknown, so we conducted further investigation into potential causes.

We carried out RNA sequencing on cerebellar vermis tissue from 12-month-old litter-matched wildtype (WT) and SCA6 mice (N=5 for each genotype) during the course of another investigation. This sequencing revealed that many genes involved in the endo-lysosomal system, as defined by the gene ontology (GO:CC) terms “Endosome” (GO:0005768) and “Lysosome” (GO:0005764), were significantly dysregulated in the SCA6 cerebellum (Fig. 1b, Padj < 0.05, see Table 1 for a full list). The expression levels of these genes were altered by between 10% and 200% in SCA6 compared to WT. Endosomal genes were found to be both up- and down-regulated in SCA6, but the genes covered by the Lysosome GO term were mostly upregulated compared to WT. The affected genes are associated with multiple endosomal compartments, meaning that the cellular consequences could be wide reaching. We therefore aimed to determine whether different compartments of the endo-lysosomal system (Fig. 1a) are altered in the cerebellum of SCA6 mice, and whether this could contribute to previously described BDNF and TrkB deficits, via mis-trafficking through the endo-lysosomal system.

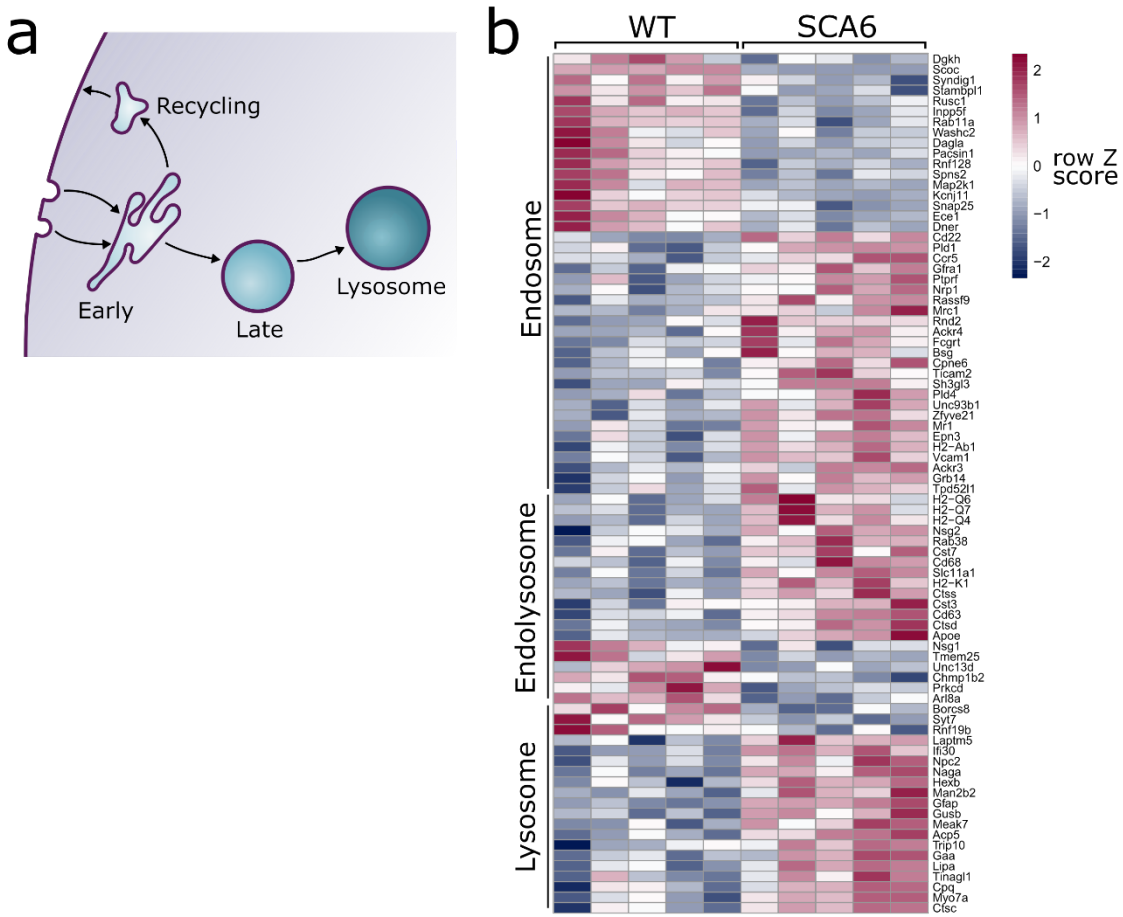

Figure 1: Endo-lysosomal genes are dysregulated in the SCA6 cerebellum.
(a) Schematic showing the endo-lysosomal system. (b) Heat map showing relative expression of endo-lysosomal associated transcripts in the cerebellum of 5 WT and 5 SCA6 mice (1 column per mouse). Genes are separated into groups based on their gene ontology categorization (GO term Endosome and Lysosome; the group “Endolysosome” denotes genes that belong to both GO term categories), only genes with an adjusted P value < 0.05 are shown.

Early endosomes are enlarged and accumulate BDNF and TrkB in Purkinje cells in SCA6 mice.

Early endosomes are the first stop for newly endocytosed cargo. There, cargo undergoes sorting as the slightly acidic pH facilitates ligand release from receptors (Fig. 2a). We carried out immunohistochemistry (IHC) against early endosome antigen 1 (EEA1) on sections of cerebellar vermis from 7–8-month WT and SCA6 mice and found that EEA1 staining is present in the cerebellum, particularly in Purkinje cells (Fig. 2b). We imaged Purkinje cells and could identify large tubular early endosomes in Purkinje cell somas of both WT and SCA6 mice (Fig. 2b, c). The early endosome marker in SCA6 Purkinje cells covered a larger area, showing that the early endosome compartment is enlarged in SCA6 (Fig. 2d). A similar enlargement of early endosomes has been seen in other neurological diseases (Cataldo et al., 2000, 1997; Jin et al., 2004). Using the EEA1 marker to delineate early endosomes, we were able to analyze BDNF and TrkB localized within the early endosome compartment. There was a higher amount of BDNF staining within the early endosomes of Purkinje cells from SCA6 mice (Fig. 2e, f). This was intriguing as we have previously shown that BDNF levels in the cerebellar vermis as a whole are decreased (Cook et al., 2022), so BDNF accumulates specifically in this compartment despite depressed levels overall in the cerebellum. We found the same was true for TrkB, as TrkB immunoreactivity was increased within the EEA1 positive early endosome compartment in SCA6 Purkinje cells compared to WT (Fig. 2g, h). Nearly all of the TrkB staining within SCA6 Purkinje cells colocalized with the EEA1 marker (Fig. 2g, arrowheads), whereas the tissue from WT mice showed abundant TrkB staining outside the early endosome compartment of Purkinje cells (Fig. 2g, arrowheads). Thus, early endosomes are enlarged and accumulate BDNF and TrkB in SCA6, despite decreased levels of both proteins in the SCA6 cerebellum as a whole. This cargo mis-trafficking could lead to a decrease in the amount of free BDNF available to signal, as well as the amount of TrkB recycled to the cell surface, thereby contributing to previously described BDNF-TrkB signaling deficits in SCA6 (Cook et al., 2022).

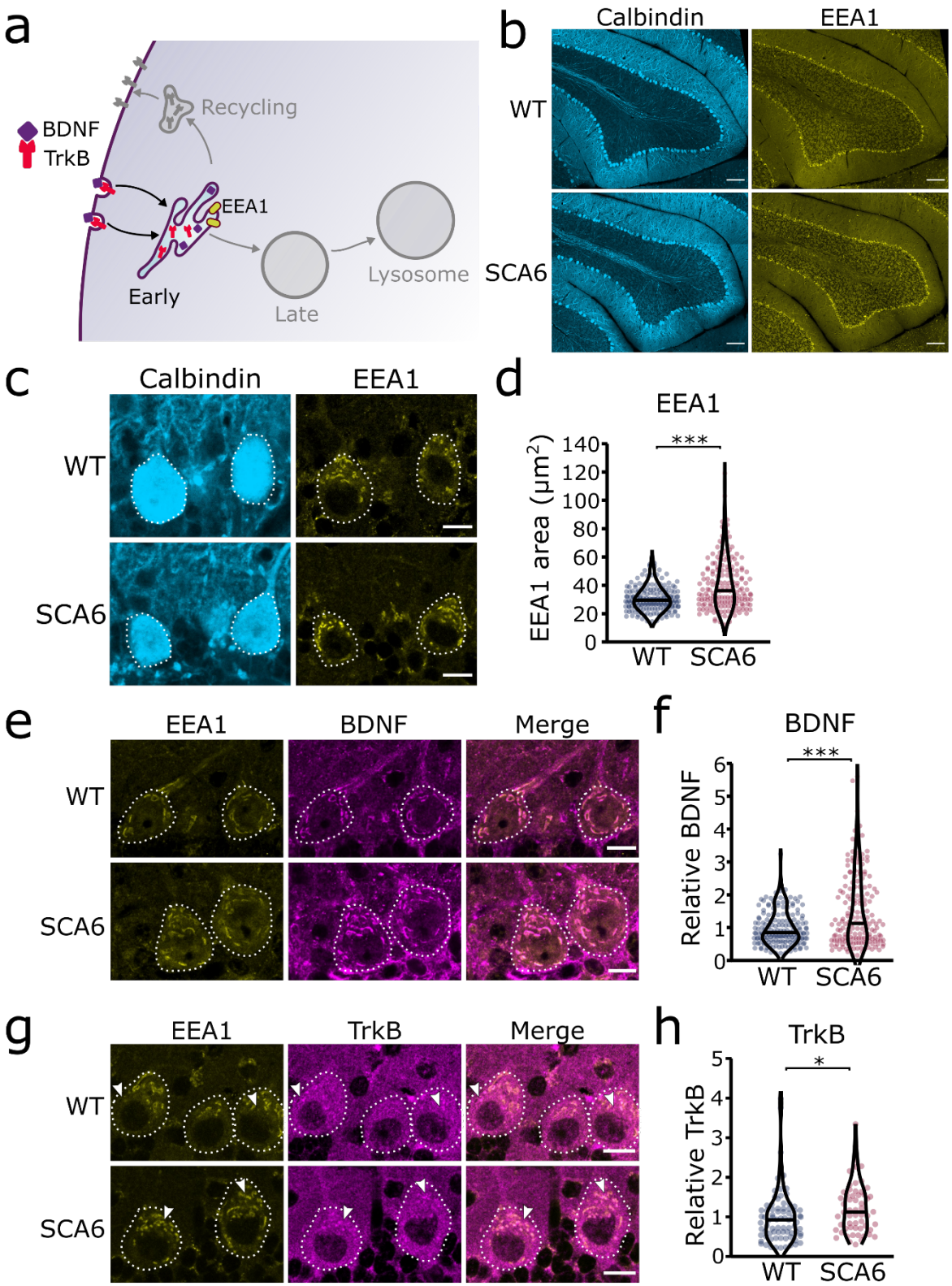

Figure 2: Early endosomes are enlarged and accumulate BDNF and TrkB in SCA6 Purkinje cells. (a) Schematic showing BDNF and TrkB endocytosis and trafficking to early endosomes labeled with EEA1. (b) The early endosome marker EEA1 stains early endosomes in lobule 3 of the cerebellar vermis in WT

143 and SCA6 mice, calbindin labels Purkinje cells. Scale bar, 100µm. (c) Closeup images of the early
144 endosome marker EEA1 in lobule 3 of cerebellum, calbindin labels Purkinje cells (outlined). Scale bar,
145 10µm. (d) The area covered by EEA1 staining in Purkinje cells is increased in SCA6 mice compared to WT
146 ($P < 0.001$; N = 6 WT mice, 173 cells; 5 SCA6 mice, 171 cells). (e) Representative images of the early
147 endosome marker EEA1 and BDNF within Purkinje cells (outlined) in the anterior vermis. Scale bar, 10µm.
148 (f) Relative staining level of BDNF within early endosome compartment is higher in the Purkinje cells of
149 SCA6 mice compared to WT ($P < 0.001$; N = 6 WT mice, 173 cells; 5 SCA6 mice, 171 cells). (g)
150 Representative images of the early endosome marker EEA1 and TrkB within Purkinje cells (outlined) in
151 the anterior vermis. Arrowheads denote locations of significant TrkB accumulations. Scale bar, 10µm. (h)
152 Relative staining level of TrkB within early endosome compartment is higher in the Purkinje cells of SCA6
153 mice compared to WT ($P = 0.013$; N = 4 WT mice, 79 cells; 4 SCA6 mice, 58 cells). Mann Whitney *U* test
154 used for all statistical comparisons, * $P < 0.05$, *** $P < 0.001$.
155
156 **Recycling endosomes are morphologically normal in SCA6.**
157 Since we identified an accumulation of TrkB in early endosomes, we wondered whether this would affect
158 the amount of TrkB recycled back to the cell surface. Recycling endosomes return receptors to the plasma
159 membrane for further signaling (Fig. 3a) (O'Sullivan and Lindsay, 2020). Syntaxin 12/13 (Stx13) is
160 involved in recycling of endocytosed proteins back to the plasma membrane and is located in recycling
161 endosomes and some tubular protrusions from early endosomes that are also involved in recycling (Prekeris
162 et al., 1998). We used two different antibodies for Stx13 as a marker for the recycling endosome
163 compartment. Staining with both antibodies revealed a large network of small recycling endosomes and
164 protrusions in Purkinje cells (Fig. 3b, Supp. Fig 1). Analysis of the staining with both antibodies showed
165 that recycling endosome area was unchanged in SCA6 Purkinje cells (Fig. 3c, Supp. Fig. 1). We noted
166 colocalization between TrkB and Stx13, showing TrkB being recycled back to the cell surface after
167 dissociation from bound BDNF in the early endosomes. The TrkB staining within the recycling endosome
168 compartment marked by Stx13 was decreased in Purkinje cells in SCA6 mice (Fig. 3d). Combined with the
169 increased levels of TrkB in the early endosomes of Purkinje cells in SCA6 (Fig. 2h), these data argue that
170 TrkB is stuck in early endosomes in SCA6, rather than being recycled to the cell surface to the same extent
171 as in WT Purkinje cells. This mislocalization may contribute to the depressed levels of BDNF-TrkB
172 signaling previously described in SCA6 (Cook et al., 2022).

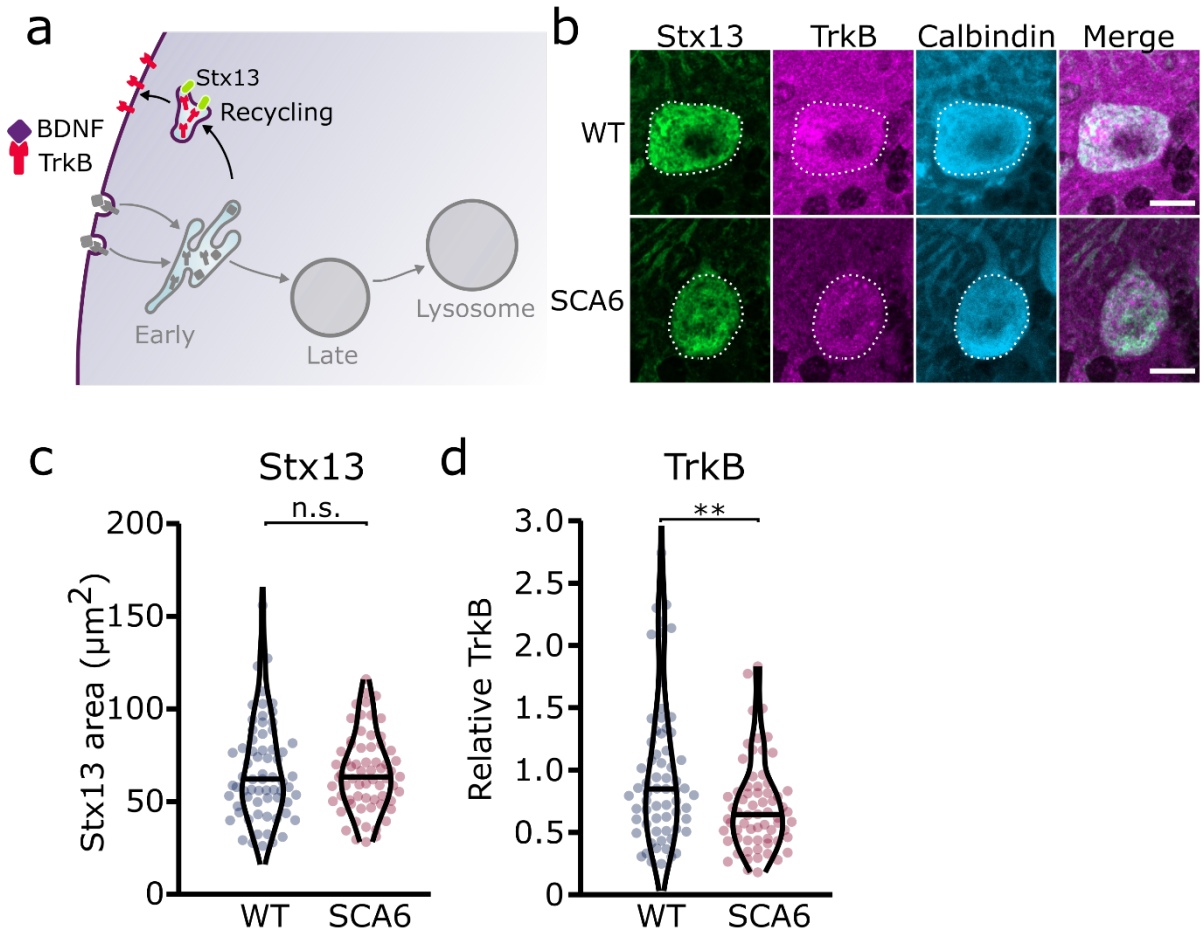

Figure 3: Recycling of TrkB in recycling endosomes is impaired in SCA6 Purkinje cells. (a) Schematic showing the return of TrkB to the cell membrane via recycling endosomes labeled with Stx13. (b) Representative images of the recycling endosome marker Stx13 and TrkB within Purkinje cells (outlined) of the anterior vermis. Scale bar, 10μm. (c) The area covered by Stx13 staining in Purkinje cells is unchanged between WT and SCA6 mice ($P = 0.96$; N = 4 WT mice, 67 cells; 4 SCA6 mice, 66 cells). (d) The relative level of TrkB within recycling endosomes was significantly decreased in SCA6 Purkinje cells ($P = 0.0034$; N = 4 WT mice, 67 cells; 4 SCA6 mice, 66 cells). Mann Whitney *U* test used for all statistical comparisons, ** $P < 0.01$, n.s. $P > 0.05$.

Late endosomes

Early endosomes undergo maturation into late endosomes in order to transport cargo destined for degradation to the lysosomes (Huotari and Helenius, 2011) (Fig. 4a). Neurons use this degradative pathway as a way to regulate BDNF levels (Evans et al., 2011). We used Rab7 as a marker for late endosomes (Vitelli et al., 1997), and identified numerous late endosomes in Purkinje cells of both WT and SCA6 mice (Fig. 4b). The Rab7 staining covered a smaller area in the Purkinje cells of SCA6 mice compared to WT (Fig. 4c), indicating a reduction in the size or number of late endosomes. Most of the BDNF staining within the Purkinje cells did not colocalize with Rab7 (Fig. 4b), which was expected as we had previously found high levels of colocalization of BDNF with the early endosome marker EEA1 (Fig. 2e). The BDNF staining that was present within the Rab7 positive late endosome compartment was significantly reduced in SCA6 compared to WT (Fig. 4d), suggesting that BDNF accumulates in the early endosomes earlier in the

endosomal pathway (Fig. 2f), preventing its progression through the late endosomal stage. Late endosomes transport cargo to lysosomes for degradation, so less BDNF may reach the lysosome in SCA6. This could have implications for the regulation of BDNF within Purkinje cells, as neurons tightly regulate BDNF levels via degradative pathways (Evans et al., 2011).

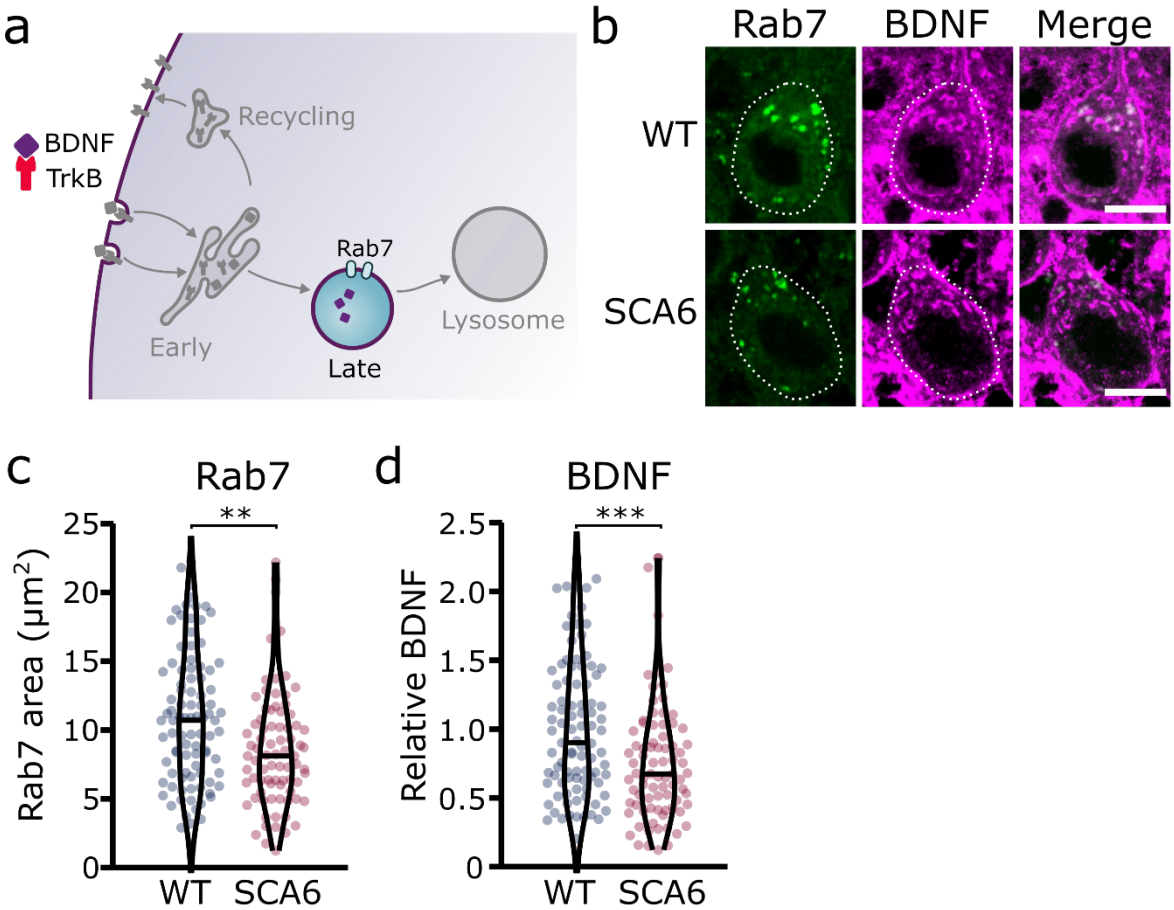

Figure 4: Late endosomes are reduced in SCA6 Purkinje cells and carry less BDNF.
(a) Schematic showing the transport of BDNF in late endosomes expressing Rab7. (b) Representative images of the late endosome marker Rab7 and BDNF within Purkinje cells (outlined) of the anterior vermis. Scale bar, 10μm. (c) The area covered by Rab7 staining in Purkinje cells is decreased in SCA6 mice compared to WT ($P = 0.0019$; N = 4 WT mice, 93 cells; 4 SCA6 mice, 81 cells). (d) The relative level of BDNF within late endosomes was significantly decreased in SCA6 Purkinje cells ($P < 0.001$; N = 4 WT mice, 93 cells; 4 SCA6 mice, 81 cells). Mann Whitney *U* test used for all statistical comparisons, ** $P < 0.01$, *** $P < 0.001$.

Lysosomal morphology is unchanged in SCA6.
We next aimed to determine whether lysosomes were altered in SCA6, using a dual strategy to visualize the lysosomes in cerebellar slices. We first used a pH sensitive dye, LysoTracker Red DND 99, to visualize the acidic lysosomes (Fig, 5a, b) (Chazotte, 2011). As LysoTracker labels all acidic compartments, it is not sufficient to confirm the identity of lysosomes. This may be particularly problematic if other intracellular compartments undergo inappropriate acidification, which has been observed in other neurological diseases (Pescosolido et al., 2021). Therefore, after staining acute cerebellar slices with LysoTracker, we performed immunohistochemistry for Lysosomal-associated membrane protein 1 (Lamp1), a glycoprotein localized at

216 the membranes of lysosomes. Because even Lamp1 can be localized outside of lysosomes (Cheng et al.,
217 2018), we used both LysoTracker and Lamp1 to identify lysosomes in Purkinje cells. We found that both
218 stains labelled lysosomes within Purkinje cells (Fig. 5b). As expected, the Lamp1 staining appeared as ring
219 like structures, marking the membranes of the lysosomes, while LysoTracker staining marked the acidic
220 lumen of the lysosomes, in the center of these rings (Fig. 5b, see zoom). While Lamp1 staining identified a
221 large number of lysosomes of varying size, the LysoTracker stain was present only in the largest. This
222 discrepancy has been noted previously, as LysoTracker does not label the smallest lysosomes in cerebellar
223 slices or other cell preparations that are fixed after staining (Chazotte, 2011; Song et al., 2008). We found
224 that the total area covered by the Lamp1 and LysoTracker stains was not significantly different between
225 Purkinje cells from WT and SCA6 mice (Fig. 5c, d). The area of colocalization between the two stains was
226 also unchanged (Fig. 5e).
227
228 To investigate further and determine whether the two stains label the same population of lysosomes in the
229 two genotypes, we counted the number of lysosomes labelled by different combinations of the two markers.
230 The lysosomes labelled by these two strategies could be divided into 3 groups. (1) Compartments stained
231 by both Lamp1 and LysoTracker, confirming that they are indeed lysosomes. The number of these
232 lysosomes was indistinguishable between WT and SCA6 mice (Fig. 5f), indicating that Lamp1 positive
233 lysosomes are present in normal quantities and are appropriately acidified in SCA6 Purkinje cells. In
234 agreement, the area covered by each stain per lysosome, a proxy for the size of the lysosomes, was
235 unchanged in SCA6 (Supp. Fig. 2). (2) Lysosomes labelled by Lamp1 but not LysoTracker (Fig. 5g)
236 represent small lysosomes unable to retain the LysoTracker dye after fixation (Chazotte, 2011; Song et al.,
237 2008). This number was not significantly different between WT and SCA6 mice and so Lamp1 appears to
238 be present at normal levels and is appropriately localized to lysosomes in SCA6. (3) Organelles labelled by
239 LysoTracker but not Lamp1 could include maturing late endosomes or other endosomal compartments that
240 are inappropriately acidified. Late endosomes have an acidic pH and Rab7 positive late endosomes can be
241 LysoTracker positive (Majzoub et al., 2016). Late endosomes fuse with lysosomes to complete cargo
242 degradation, but first they mature into an intermediate compartment called an endolysosome (Huotari and
243 Helenius, 2011). Therefore, these LysoTracker-positive Lamp1-negative organelles could be late
244 endosomes or intermediate endolysosomes that have not yet fused with the Lamp1 positive lysosomes. The
245 number of these compartments was low in Purkinje cells in both genotypes but was significantly lower in
246 SCA6 mice (Fig. 5h). This agrees with our finding of a reduction in the size of the late endosome
247 compartment in SCA6 mice (Fig. 4c). A reduction in the late endosome compartment suggests that there
248 are fewer late endosomes available to mature and fuse with lysosomes. Therefore, the Lamp1 positive
249 lysosomes are morphologically normal in the Purkinje cells of SCA6 mice while the small alteration in
250 Lysotracker staining likely represents a deficit in the maturation of late endosomes before fusion with
251 lysosomes.

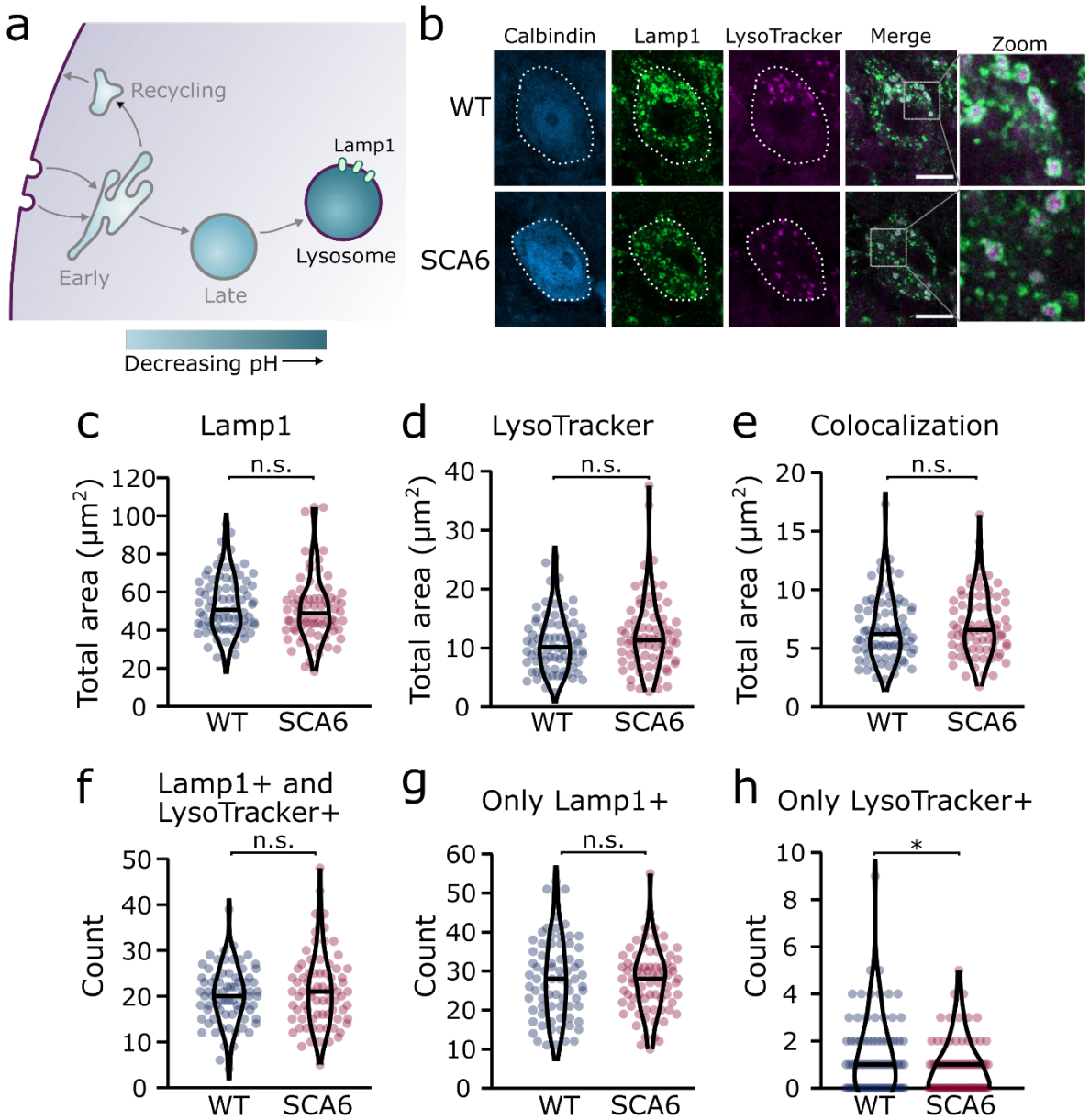

Figure 5: Lysosomes in SCA6 Purkinje cells are morphologically normal but there may be a deficit in late endosome maturation.

(a) Schematic showing the endo-lysosomal system as a series of compartments of increasingly acidic pH with lysosomes, expressing Lamp1, being most acidic. (b) Representative images of Purkinje cells in the anterior vermis stained for the lysosome membrane marker Lamp1 and LysoTracker as a marker of acidic compartments. Calbindin labels Purkinje cells (outlined). Scale bar, 10μm. The area covered by (c) Lamp1 staining and (d) LysoTracker staining in Purkinje cells is unchanged between WT and SCA6 mice (P = 0.26 for Lamp1; P = 0.20 for LysoTracker; N = 3 WT mice, 78 cells; 3 SCA6 mice, 76 cells). (e) The area of colocalization between Lamp1 and Lysotracker is unchanged between WT and SCA6 mice (P = 0.34; N = 3 WT mice, 78 cells; 3 SCA6 mice, 76 cells). (f) The number of lysosomes that were both Lamp1 positive and LysoTracker positive was not significantly different between genotypes (P = 0.72; N = 3 WT mice, 78 cells; 3 SCA6 mice, 76 cells). (g) The number of lysosomes that were Lamp1 positive, but LysoTracker

negative was unchanged between genotypes (P = 0.83; N = 3 WT mice, 78 cells; 3 SCA6 mice, 76 cells). (h) The number of putative late endosomes undergoing maturation that were Lamp1 negative, but LysoTracker positive was significantly decreased in the Purkinje cells of SCA6 mice (P = 0.034; N = 3 WT mice, 78 cells; 3 SCA6 mice, 76 cells). Mann Whitney *U* test used for all statistical comparisons except number of Lamp1+ puncta (f) which was normally distributed and so a Student's *t* test was used, * P < 0.05, n.s. P > 0.05.

Taken together, these results suggest that although lysosomes are present in normal numbers, the trafficking of endocytosed cargo to the lysosome for degradation is impaired in the SCA6 cerebellum. Our transcriptomic data furthermore shows that genes encoding lysosomal proteins are abnormally expressed in SCA6 (Fig. 1b), suggesting that lysosomal dysfunction is present in SCA6. Lysosomes are enzymatically active sites of degradation and contain multiple proteases that rapidly break down proteins. However, lysosomal proteolysis depends not just on enzymatic activity, but on the correct transport of proteins to the lysosomes through endosomal compartments. We wondered whether the deficits we identified in early and late endosomes (Fig. 2, 4), or other deficits in lysosome activity, might impair the ability of lysosomes to degrade endocytosed cargo in SCA6. We assayed this by incubating acute cerebellar slices with BODIPY FL Pepstatin A, an exogenous peptide that can be endocytosed and transported to the lysosome, where it binds to the active form of the lysosomal enzyme Cathepsin D (Chen et al., 2000) (Fig. 6a). We could visualize Pepstatin A signal within Lamp1 positive puncta, demonstrating Cathepsin D enzymatic activity within lysosomes (Fig. 6b). The Pepstatin A signal within Purkinje cells was significantly reduced in SCA6 mice (Fig. 6c, d), revealing a lower level of either the endocytosed construct, or of active Cathepsin D. The identification of alterations in the early and late endosomes that transport cargo to the lysosomes (Fig. 2, 4), suggests that SCA6 Purkinje cells have endosomal deficits that reduce transport of the endocytosed Pepstatin A construct to the lysosome where it can bind active Cathepsin D. This finding is therefore consistent with an overall impairment of endo-lysosomal trafficking. The reduction in Pepstatin A signal would also be consistent with a reduction in Cathepsin D enzymatic activity that could further contribute to aberrant handling of endocytosed cargo in SCA6. RNA-sequencing identified an upregulation of lysosomal enzyme transcripts in the SCA6 cerebellum, including the *CTSD* gene encoding Cathepsin D (Fig. 1b). However, this would not necessarily lead to an increase in enzyme activity as the RNA must first be translated, and then undergo post-translational proteolytic processing in order to produce the active form of Cathepsin D that binds Pepstatin A (Zaidi et al., 2008). This suggests that in SCA6, there is an upregulation in *CTSD* and other lysosomal genes that does not lead to an increase in functional enzymes. This may be a compensatory mechanism for trafficking deficits of cargoes to the lysosomal compartment, or an attempt to compensate for deficits in the production of the active form of Cathepsin D. In summary, our results illustrate that Purkinje cells in SCA6 mice have an impaired ability to degrade other endocytosed cargo beyond BDNF and TrkB. This likely arises from trafficking deficits that result in a disruption in the transport of cargo to the lysosomes, along with lysosomal dysfunction.

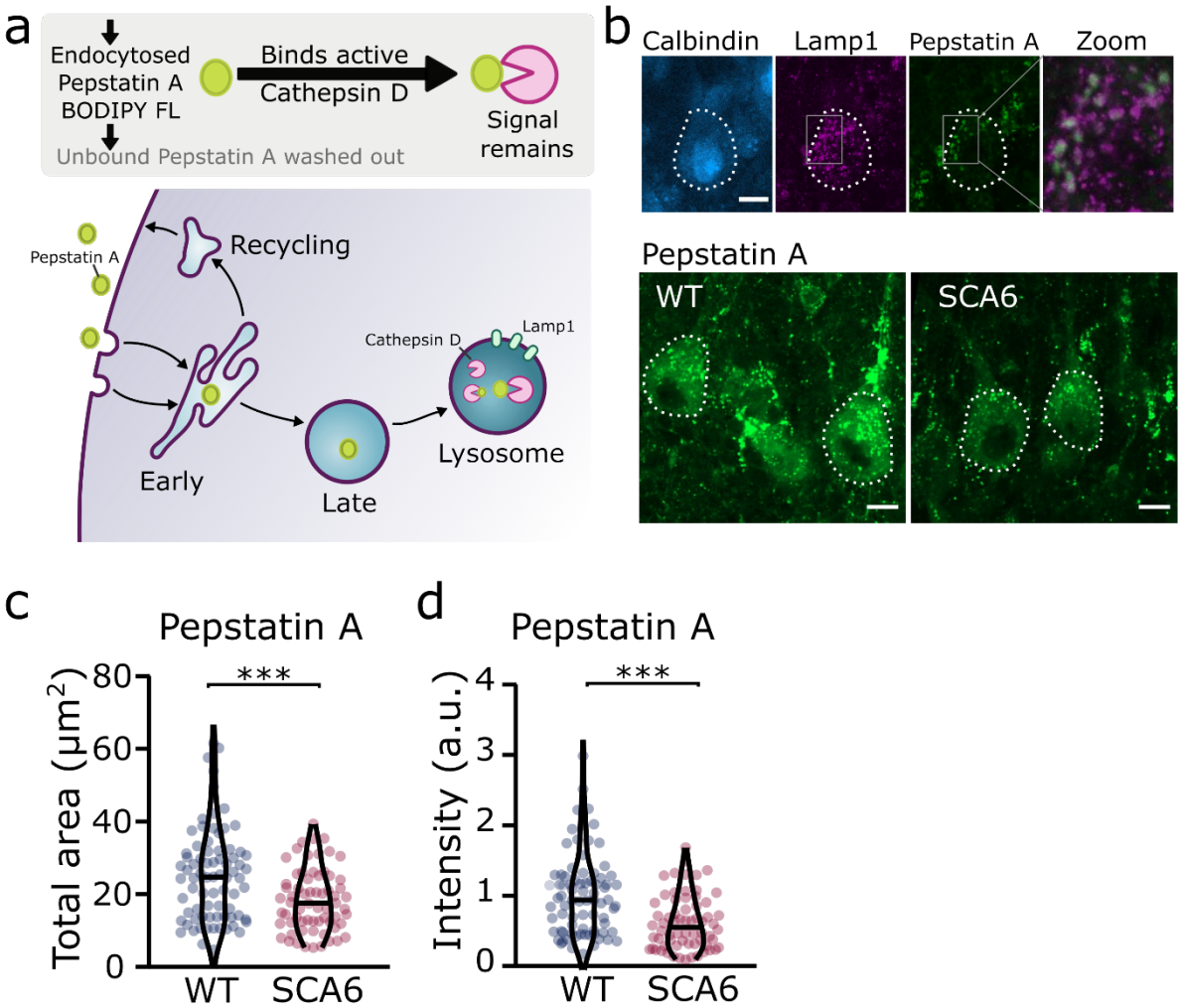

Figure 6: Trafficking of an exogenous peptide to the lysosome shows impairment in lysosomal action on endocytosed cargo in SCA6.
(a) Schematic showing the use of Pepstatin A BODIPY FL construct to visualize endosome trafficking and Cathepsin D activity. (b) Representative images of Pepstatin A staining in the anterior vermis. Top row shows colocalization with lysosome marker Lamp1, Calbindin labels Purkinje cells (outlined). Scale bars, 10μm (c) The area covered by Pepstatin A staining in Purkinje cells was significantly decreased in SCA6 mice ($P = 0.00076$; N = 3 WT mice, 78 cells; 3 SCA6 mice, 66 cells). (d) The intensity of Pepstatin A staining within Purkinje cells was significantly decreased in SCA6 mice ($P < 0.0001$; N = 3 WT mice, 78 cells; 3 SCA6 mice, 66 cells). Mann Whitney *U* test used for all statistical comparisons, *** $P < 0.001$.

7,8-DHF rescues deficits in early endosomes

We have previously shown that the putative TrkB agonist 7,8-DHF increases TrkB expression and activates Akt signaling downstream of TrkB, leading to a rescue of deficits in motor coordination and Purkinje cell firing in SCA6 mice (Fig. 7a) (Cook et al., 2022). One interpretation of this rescue is that the TrkB agonist compensates for reduced levels of BDNF in the SCA6 cerebellum, thereby activating downstream signaling cascades to restore cerebellar function. However, we have also previously shown that TrkB activation with 7,8-DHF led to increased levels of TrkB in the SCA6 cerebellum (Cook et al., 2022), suggesting that self-

amplification of TrkB signaling may play a role in the rescue. 7,8-DHF may therefore not be simply replacing lost BDNF in SCA6. Indeed, there is some evidence that 7,8-DHF may act via antioxidant or anti-inflammatory effects independent of TrkB activation (Chen et al., 2011; Han et al., 2014; Park et al., 2012). Given that TrkB signaling is known to be involved in the regulation and trafficking of endosomes (Scott-Solomon and Kuruvilla, 2018), we wondered whether chronic oral administration of 7,8-DHF to SCA6 mice would rescue the deficits in early endosome size, either due to TrkB activation or another mechanism of action. We used the same treatment regimen of 7,8-DHF that had previously been shown to rescue deficits in behaviour and Purkinje cell firing, which comprised of 1 month of oral administration of the drug to peri-onset (6–7-month-old) SCA6 mice (Fig 7a). Half of the mice received control solution with no drug added. After one month of 7,8-DHF administration, cerebellar vermis sections were stained for BDNF and EEA1 as an early endosome marker, as previously described (Fig. 2). 7,8-DHF administration rescued the size of the early endosomes, with the total EEA1 area within Purkinje cells reducing to the WT level previously described (Fig. 7b, c). The level of BDNF accumulation within the early endosomes was also restored (Fig. 7d), suggesting that in addition to self-amplifying upregulation of TrkB (Cook et al., 2022), treatment with 7,8-DHF can normalize intracellular localization and trafficking of BDNF, consistent with the role of TrkB in regulating endosome trafficking and function (Scott-Solomon and Kuruvilla, 2018).

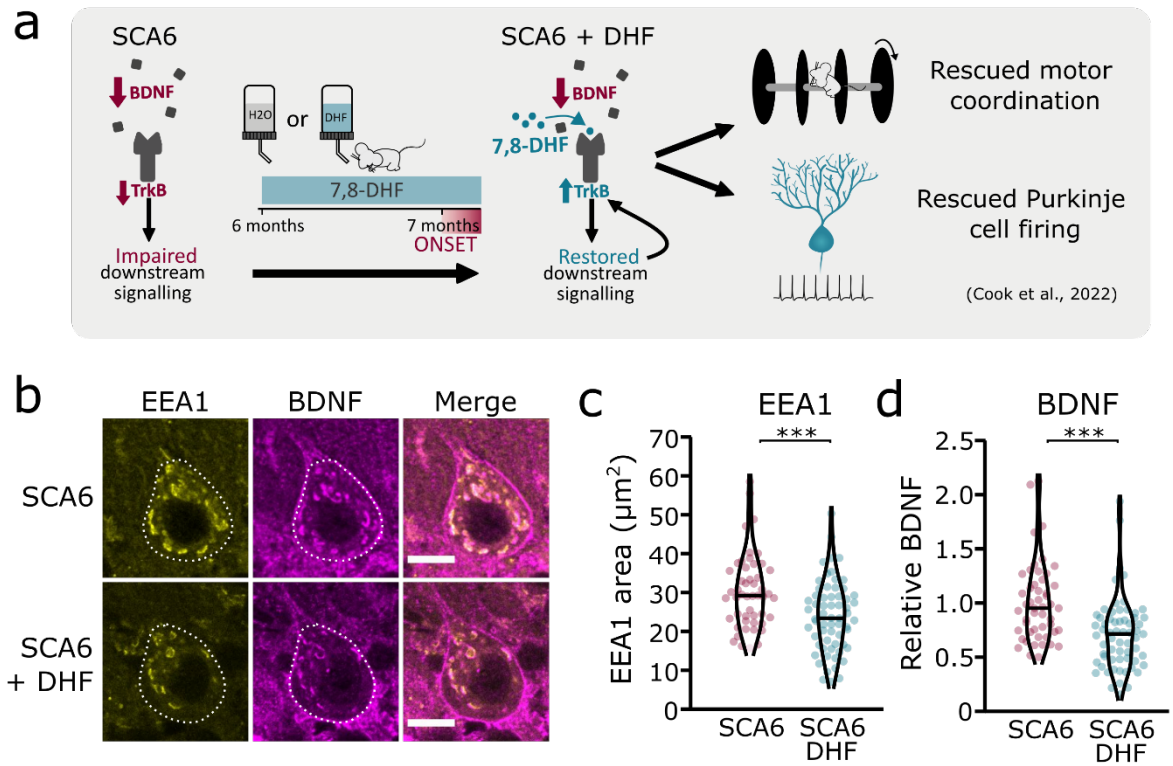

Figure 7: TrkB activation with 7,8-DHF rescues early endosomes deficits in SCA6 Purkinje cells. (a) Schematic showing 7,8-DHF administration to SCA6 mice and the previously described therapeutic benefits of 7,8-DHF in SCA6 mice. (b) Representative images of the early endosome marker EEA1 and BDNF within Purkinje cells (outlined) of the anterior vermis. Scale bar, 10μm. (c) The area covered by EEA1 staining in Purkinje cells is decreased in SCA6 mice given DHF compared to those that received control water ($P < 0.001$; Student's *t* test; N = 3 SCA6 mice, 50 cells; 3 SCA6 DHF mice, 63 cells). (d) Relative staining level of BDNF within early endosome compartment is decreased in the Purkinje cells of

SCA6 mice that received DHF compared to controls (P < 0.001; Mann Whitney *U* test; N = 3 SCA6 mice, 50 cells; 3 SCA6 DHF mice, 63 cells). *** P < 0.001.

Discussion

We have identified multiple novel deficits in the endo-lysosomal pathway that could contribute to BDNF-TrkB signaling alterations in SCA6 (Fig. 8). Early endosomes were enlarged in SCA6 and accumulate BDNF and TrkB. Recycling endosomes were morphologically normal but carried less TrkB, and late endosomes were reduced in size and carried less BDNF. This suggests that cargo is getting stuck in the enlarged early endosomes in SCA6. The involvement of lysosomal pathology in SCA6 is less clear. Lysosomes appear morphologically normal with normal pH, but RNA-sequencing revealed upregulation of lysosomal genes in SCA6. SCA6 Purkinje cells also showed a reduction in exogenous cargo binding to the lysosomal enzyme Cathepsin D, indicating either a deficit in lysosomal enzyme activity, defects in endocytosis and cargo trafficking to lysosomes, or both. Taken together, these deficits could lead to cellular dysfunction in SCA6. This work further highlights how BDNF and TrkB deficits manifest in SCA6, and the potential of targeting this pathway therapeutically.

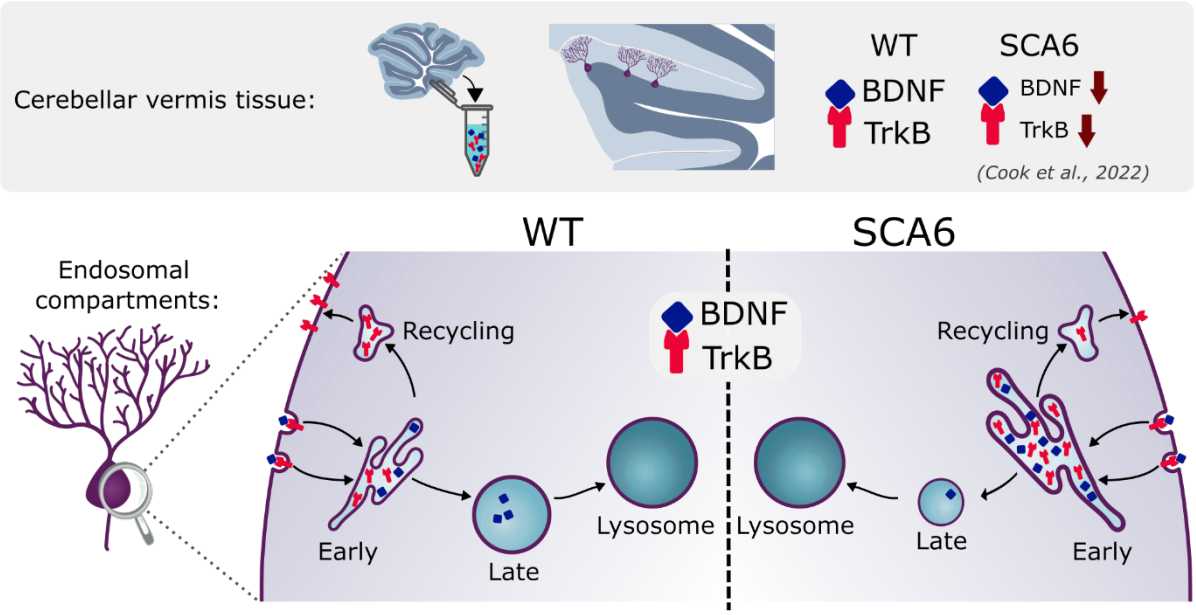

Figure 8: Multiple deficits in the endo-lysosomal system lead to abnormal localization of BDNF and TrkB in the Purkinje cells of SCA6 mice.

Excitingly, both the enlargement of early endosomes and the accumulation of BDNF in early endosomes could be rescued by the putative TrkB agonist, 7,8-DHF. There is evidence that TrkB can regulate its own expression and signaling (Cheng et al., 2011; Haapasalo et al., 2002) and we had previously shown that 7,8-DHF administration increased levels of TrkB in the cerebellum of SCA6 mice (Cook et al., 2022). This new finding demonstrates that not only does 7,8-DHF regulate the expression of TrkB in the SCA6 cerebellum, but also the localization of the ligand for TrkB within endosomal compartments, providing insight into the mechanisms by which BDNF and TrkB are regulated in the cerebellum. Furthermore, the finding that 7,8-DHF can rescue endosomal deficits in SCA6 supports the promise of 7,8-DHF and related

376 molecules as potential therapeutics for SCA6 and raises the possibility of their use for treatment of other
377 disorders displaying early endosome deficits.
378
379 Early endosome deficits are not unique to SCA6, meaning that this finding may have a wider application.
380 Enlargement of early endosomes is a hallmark of dysfunction in the endosomal pathway (Kaur and
381 Lakkaraju, 2018) and has been observed in multiple diseases including Alzheimer's disease (Cataldo et al.,
382 2004, 2000, 1997; Tate and Mathews, 2006), Down syndrome (Cataldo et al., 2000), models of macular
383 degeneration (Kaur et al., 2018), Charcot-Marie-Tooth (Bucci et al., 2012) and Parkinson's disease
384 (Vidyadhara et al., 2019). Early endosome abnormalities can arise from deficits in maturation or fusion of
385 early endosomes, or alterations in the microtubule networks that govern endosome fusion (Skjeldal et al.,
386 2012). Purkinje cells may be particularly susceptible to early endosome enlargement, as in postmortem
387 tissue from Niemann Pick type C patients, Purkinje cells had enlarged early endosomes which accumulated
388 amyloid precursor protein, whereas in the hippocampus, pathology mostly concerned late endosomes (Jin
389 et al., 2004). However, endosomal pathology in SCA6 and other diseases is not limited to early endosomes,
390 and other endosomal compartments can be targeted therapeutically (Bonam et al., 2019; Tate and Mathews,
391 2006). In addition to identifying TrkB activation as a therapeutic strategy for endosome deficits, our work
392 opens the door for the development of additional endosome-targeting treatment strategies for SCA6.
393
394 Our findings provide the first evidence for endosomal dysfunction contributing to signaling deficits in
395 spinocerebellar ataxias. Other ataxias like SCA1 also have reduced BDNF protein levels (Mellesmoen et
396 al., 2019), so it would be interesting to determine whether early endosome deficits could contribute to
397 disrupted BDNF signaling in other ataxias. Polyglutamine diseases in general are thought to have disruption
398 in protein degradation pathways (Chai et al., 1999; Cortes and La Spada, 2015), and SCA7 patients and
399 mouse models display alterations in lysosome pathways (Alves et al., 2014). Therefore, similar
400 abnormalities could be a common feature of similar diseases.
401
402 There remain, however, some unanswered questions from our study. What is the specific deficit that leads
403 to early endosome enlargement and other deficits? Is it the same as in other neurological diseases? Future
404 work to identify this will further aid in the development of endosome-targeting therapies. There is also the
405 question of the effect on other cargo. Sorting and recycling happens in a cargo-specific manner (Hu et al.,
406 2015) and so other cargo could be handled differently. Here we investigated endosomal trafficking of
407 BDNF and TrkB as we have previously shown this pathway to be both dysregulated in SCA6, and amenable
408 to therapeutic targeting. However, our experiments with BODIPY FL Pepstatin A suggest that even
409 exogenous cargo could be transported differently in SCA6. Future research should consider whether other
410 cargo accumulate in early endosomes and how this affects cell physiology. Furthermore, in parallel to
411 endocytosis and endosome trafficking, cells transport proteins for degradation in lysosomes via autophagy
412 (Klionsky, 2005). There are therefore two pathways with a common destination of degradation in
413 lysosomes, both of which are important for cell function, and abnormalities in one pathway can lead to
414 disruption in the other (Birgisdottir and Johansen, 2020; Mahapatra et al., 2019). Future work should
415 therefore investigate whether autophagy is disrupted in SCA6. Finally, while most of our study was
416 conducted around disease-onset, the transcriptomic alterations were measured at a later timepoint, which
417 raises the question of whether transcriptional changes drive endo-lysosomal alterations or are in fact a result
418 of endo-lysosomal changes that are caused by a different mechanism. A careful study of the timeline of
419 these changes will help us understand the sequence of events as disease progresses in SCA6.

420 In summary, we have identified a dysregulated cellular trafficking pathway that contributes to cerebellar
421 pathophysiology that is novel not just in SCA6, but in SCAs in general. We found that several components
422 of the endo-lysosomal system show abnormalities in Purkinje cells in SCA6 mice. These deficits could
423 contribute to BDNF-TrkB signaling deficits in SCA6, as BDNF and TrkB accumulate in early endosomes

424 and there is a reduction in TrkB being recycled to the cell membrane for further signal transduction. The
425 endo-lysosomal system is therefore a promising therapeutic target for SCA6.
426
427 ## Methods
428 ### Animals
429 As previously described, the SCA6$^{84Q/84Q}$ mouse model is a knock-in mouse with a humanized 84 CAG
430 repeat expansion mutation at the *CACNA1A* locus (Jayabal et al., 2015; Watase et al., 2008). We bred
431 heterozygous mice to generate SCA6$^{84Q/84Q}$ and litter-matched WT control mice. Breeding mice were
432 originally purchased from Jackson laboratories (Bar Harbor, Maine; strain: B6.129S7-Cacna1atm3Hzo/J;
433 stock number: 008683) and primer sequences for genotyping were provided by Jackson laboratories. This
434 breeding setup allowed us to use experimental cohorts that contained litter- and sex-matched mice randomly
435 assigned to experimental groups. Both male and female mice were included in all experiments, and we did
436 not exclude any experimental animals from analysis. The only experiment that included pre-selection of
437 mice was for RNA Sequencing where mice were selected for tissue collection based on rotarod
438 performance, to include animals that were representative of their genotype. For all other experiments mice
439 were selected at random and none were excluded. Animal husbandry and procedures were approved by the
440 McGill Animal Care Committee in accordance with the Canadian Council on Animal Care guidelines. All
441 staining experiments were carried out on tissue from mice aged 7-8 months of age, except the Lamp1 and
442 Lysotracker staining which was carried out at 12 months of age.
443
444 ### RNA extraction and sequencing
445 RNA extraction was performed on tissues from 5 WT (2 male, 3 female) and 5 SCA6 (3 male, 2 female)
446 mice at 12 months of age. Experimental mice were selected based on rotarod performance in order to
447 identify mice that were phenotypically representative of their genotype. The experimental area and tools
448 were cleaned with RNAseZap (Sigma #R2020) to remove RNAse contamination prior to starting
449 experiments. Mice were anesthetised with isoflurane until the loss of toe pinch reflex, decapitated and the
450 cerebellar vermis was dissected, separated into anterior and posterior sections, flash frozen on dry ice, and
451 stored at -80°C until RNA extraction. RNA extraction proceeded as follows, with all procedures carried out
452 on ice or at 4°C. Cerebellar vermis tissue sections were mechanically homogenized in TRIzol reagent
453 (Invitrogen #15596026) by passing the lysate repeatedly through a series of needles, starting at 18-gauge,
454 followed by 23-gauge. Chloroform (Sigma #288306) was added to the homogenate to separate total RNA
455 in the aqueous phase, and RNA was recovered by precipitation with ethanol (70%). RNA extracts were
456 purified using the RNeasy Mini Kit (Qiagen #74104) with DNase I treatment as described in the
457 manufacturer's protocol.
458
459 The RNA integrity of samples was quantified with capillary electrophoresis (Agilent BioAnalyzer 2100) in
460 order to generate an RNA integrity number (RIN). All samples had an RIN over 7.5 and therefore were
461 assessed to have high RNA quality. Library preparation and sequencing was carried out by Genome Quebec
462 (Montreal, Quebec, Canada) using NEB stranded mRNA library prep, sequenced on the Illumina NovaSeq
463 6000 S4 generating 100bp paired-end reads. Samples had a median of 53 million reads (IQR, 42-64 million
464 reads), and a median of 92% mapping rate (IQR, 92%-92%).
465
466 ### RNA sequencing data analysis
467 The generated FASTQ files were transferred to the Digital Research Alliance of Canada cloud server for
468 processing and analysis. First, reads were aligned to the mouse reference genome (GRCm38) using HISAT2
469 version 2.1.0 (Kim et al., 2019). Quantification of reads was carried out with HTSeq version 0.11. (Anders
470 et al., 2015) in union mode. Reads generated from anterior and posterior samples were combined by

471 addition at this step to generate an *in silico* whole cerebellar vermis read count. Differential expression
472 analysis was performed with DESeq2 version 1.24.0 in RStudio (Love et al., 2014). DESeq2 adjusted P
473 values for multiple testing with a target $\alpha = 0.05$, and genes were considered to be differentially expressed
474 genes (DEGs) at FDR < 0.05. Enriched gene pathways were identified using gProfiler (Raudvere et al.,
475 2019) based on terms in gene ontology (GO) databases.
476
477 **Immunohistochemistry**
478 Tissue sections for immunohistochemistry (IHC) were prepared as described previously (Cook et al., 2022).
479 Mice were deeply anesthetised with 400mg/kg 2,2,2-tribromoethanol (Avertin) prepared in sterile 0.85%
480 saline for a working concentration of 20mg/ml. Intracardiac perfusion comprised of a flush with 40mL of
481 heparin in phosphate-buffered saline (PBS; 0.1 M, pH 7) followed by 40mL of 4% paraformaldehyde in
482 phosphate buffer (PB). Brains were rapidly removed and incubated in 4% PFA for a further 24 hours of
483 fixation at 4°C on an orbital shaker at 70RPM. Brains were dissected to separate the cerebellum and sliced
484 using a vibrating microtome (5100mz Vibrotome, Campden Instruments, Loughborough, UK) into sections
485 of 75 or 100µm thickness. Slices were kept at 4°C in PBS with 0.05% sodium azide to inhibit microbial
486 growth before staining.
487
488 Free-floating slices were rinsed with PBS and incubated in primary antibody (Table 2) and blocking
489 solution with BSA for 3 days, then rinsed in PBS and incubated for 90 minutes with secondary antibodies
490 (Table 2). For experiments involving anti-mouse secondary antibodies, an additional incubation with Fab
491 fragments (AffiniPure Fab Fragment Anti-Mouse IgG, Jackson Immunoresearch 715-007-003) was added
492 prior to secondary antibody incubation. After a final PBS wash, stained slices were mounted using ProLong
493 Gold Antifade mounting medium (Thermo Fisher Scientific, Waltham, USA) and stored at 4°C and
494 protected from light prior to imaging.
495
496 As previously described, we found that the anti-BDNF antibody required epitope retrieval procedures to be
497 carried out prior to staining in order to obtain adequate staining. We additionally found that epitope retrieval
498 enhanced staining with anti-EEA1. Epitope retrieval took the form of a heat-induced epitope retrieval
499 (HIER) step involving heating the slices in PBS to 95°C for ten minutes immediately prior to staining.
500 Slices were allowed to cool and IHC procedures were carried out as normal. This greatly enhanced the
501 quality of BDNF and EEA1 staining and allowed us to resolve intracellular endolysosomal structures in
502 Purkinje cells (Supp. Fig. 3). HIER did not affect the staining of Purkinje cells with anti-calbindin (Supp.
503 Fig. 3) and so the effect was specific to certain antigens and antibodies and not to the tissue in general.
504
505 To further validate BDNF staining, we used liver tissue as a negative control. In rodent liver, the majority
506 of tissue contains very low levels of BDNF (Koppel et al., 2009; Vivacqua et al., 2014), except from some
507 BDNF-expressing cholangiocytes (Vivacqua et al., 2014). We therefore used liver tissue from a WT mouse
508 undergoing surgery for another project as a negative control to validate the BDNF antibody. The liver was
509 recovered from the mouse during a terminal surgery and immediately placed into 4% paraformaldehyde in
510 phosphate buffer (PB) for fixation. After 45 minutes of fixation the liver was sectioned into 100µm slices
511 using a vibrating microtome (5100mz Vibrotome, Campden Instruments, Loughborough, UK). These slices
512 underwent HIER and BDNF staining as previously described. As expected, the majority of the liver tissue
513 did not show BDNF immunoreactivity and we were able to detect putative cholangiocytes that were BDNF-
514 positive as previously described (Supp. Fig. 3).
515
516 To validate TrkB staining and confirm localization, a second TrkB antibody was used (Supp. Table 2 for
517 antibody information). We used cerebellar vermis tissue from a WT mouse to carry out TrkB staining using

two different antibodies in the same batch and with all other reagents unchanged. We found that although the alternative antibody did not have as strong signal to noise ratio (Supp. Fig. 4), the TrkB staining displayed a similar localization and both antibodies were able to label TrkB in early endosomes within Purkinje cells.

Purkinje cells sometimes contained auto-fluorescent granules that were visible under excitation from a 561nm or 488 nm laser even without primary antibody incubation (Supp. Fig. 5). In order to ascertain that these granules were not interfering with the identification of endosomes or lysosomes, staining batches included a negative control slice from each animal where applicable. These slices underwent all of the usual blocking steps except primary antibodies were not added, while secondary antibody incubation and mounting proceeded as usual. In the case of the Pepstatin A negative controls, slices were incubated in ACSF without Pepstatin A BODIPY FL, and all other steps proceeded as usual. We found that although there was some background fluorescence signal in Purkinje and other cells, the intensity of the signal was lower than the staining from the antibodies of interest and was unlikely to interfere significantly with image analysis. This can be seen in side-by-side comparisons of raw images from the same mice in Supplementary figure 5.

Lysotracker

Lysotracker staining was carried out on acute cerebellar slices. Mice were anesthetised with isoflurane until the loss of toe pinch reflex and then were decapitated into ice cold artificial cerebrospinal fluid (ACSF: 125 mM NaCl, 2.5 mM KCl, 2 mM CaCl2, 1 mM MgCl2, 1.25 mM NaH2PO4, 26 mM NaHCO3, and 20 mM glucose, bubbled with 95% O2 and 5% CO2 (carbogen) to maintain pH at 7.3; osmolality ~316 mOsm). The brain was removed and dissected, and the cerebellar vermis was sectioned into 150µm sagittal slices using a VT 1200S vibratome (Leica Microsystems, Wetzlar, Germany) in ice cold ACSF. Slices were transferred to a slice chamber filled with 37°C ACSF bubbled with carbogen for 40 minutes before staining. Slices were then incubated in LysoTracker™ Red DND-99 (ThermoFisher L7528) that was dissolved in room temperature ACSF at a concentration of 1:3000. Incubation occurred at room temperature on an orbital shaker at 70RPM. After 5 minutes of incubation the slices were transferred to 4% PFA in PB for post-fixation at 70RPM for one hour. Slices were then washed in PBS and prepared for immunohistochemistry as outlined above.

Pepstatin A

Pepstatin A imaging was carried out on acute cerebellar slices prepared in the same way as for the Lysotracker imaging outlined above. After slices were kept in 37°C ACSF bubbled with carbogen for 40 minutes they were incubated in Pepstatin A fl BODIPY (Thermofisher P12271) that was prepared at a concentration of 1µg/ mL in room temperature ACSF. A stock solution of 1µg/ 1µl pepstatin A in DMSO was prepared, to improve solubility, giving a final concentration of 0.001% DMSO in the incubation solution. Incubation lasted 30 minutes at room temperature on an orbital shaker at 70 RPM. Slices were then rinsed twice with PBS and transferred to 4% PFA for post-fixation at 70RPM for 30 minutes. Slices either underwent further staining with immunohistochemistry for Lamp1 and calbindin or were mounted onto slides immediately using ProLong Gold Antifade mounting medium (Thermo Fisher Scientific, Waltham, USA) and stored at 4°C and protected from light.

Image acquisition

Imaging was performed using an LSM800 confocal microscope (Zeiss) equipped with Zen Blue software. Images were acquired using 63x and 40x objectives at 1024 x 1024-pixel resolution. Imaging was carried out by an experimenter who was blinded to the experimental condition of the slides. All imaging and

analysis was carried out in lobule 3 of the anterior vermis, a region of the cerebellum that we have previously shown to display cellular deficits in SCA6 (Cook et al., 2022; Jayabal et al., 2015).

Image Analysis

Image analysis was performed in FIJI (ImageJ; US National Institutes of Health) (Rueden et al., 2017; Schindelin et al., 2012). Purkinje cell bodies were delineated by hand using calbindin or BDNF as a marker so that the Purkinje cell soma area could be isolated for further analysis. To calculate the area of the endosomes or lysosomes, an Otsu thresholding function of the endosomal marker was used. Despeckle and watershed functions were applied to create a region of interest consisting of the relevant endosomal compartment within the cell. These regions were used to calculate the size of different compartments, and in the analysis of lysosomes the area of colocalization between regions of interest was calculated. The regions of interest delineated with various markers were subsequently used as a mask to measure fluorescence intensity levels of the cargo of interest. The cargo level was calculated using the integrated density measurement in ImageJ within the region of interest delineating the compartment of interest, and all values were normalized to the mean WT value. In figure 6 values were normalized to the mean SCA6 control value. Analysis was carried out using custom ImageJ macros alongside manual verification.

For additional analysis of the lysosomes, we performed manual counts of Lamp1 and Lysotracker positive organelles within individual Purkinje cells.

To improve the legibility of figure panels, linear adjustments of the brightness and contrast were applied to some representative image sets. Adjustments were kept to a minimum and identical adjustments were applied to images from all conditions, occurring after image analysis. Image analysis was performed on raw images by an experimenter blinded to the experimental condition of the slides.

7,8-DHF administration

7,8-dihydroxyflavone (7,8-DHF) administration was carried out as previously described (Cook et al., 2022), as we had previously found this treatment regimen to be both well tolerated and effective at restoring TrkB-Akt signaling in SCA6 mice. Briefly, single-housed mice were provided with ad libitum access to drug solutions in place of their drinking water for 1 month. These solutions contained either 157.3 µM 7,8-DHF (TCI America) dissolved in 0.04% DMSO vehicle (Sigma, Oakville, ON, Canada) or 0.04% DMSO only as a control, dissolved in autoclaved water with 10% sucrose (Sigma, Oakville, ON, Canada) added to make the solutions palatable and disguise any taste of the drug. Solutions were prepared fresh at least twice weekly and replenished daily. It has been shown by us and others that oral administration of 7,8-DHF is sufficient to induce signaling changes in the brain (Cook et al., 2022; Gao et al., 2016; Johnson et al., 2012; Liu et al., 2016; Parrini et al., 2017; Zhang et al., 2013) and the drug has been shown to be orally bioavailable (Liu et al., 2013).

Statistical analysis

Pairwise statistical comparisons were carried out to identify statistical differences between groups. In cases where the data were normally distributed, Student's *t* tests were used, otherwise Mann Whitney *U* tests were used. The type of statistical test and the sample size is indicated in the figure legend for each plot. All violin plots show individual cells as data points, with the median displayed as a horizontal line.

612

613 **Table 1: List of DEGs in Endosome and Lysosome pathways**

Gene Name	Gene ID	Base Mean	Log2 Fold Change	Adjusted P value
H2-K1	ENSMUSG00000061232	8985.033	0.557	< 0.001
Cst7	ENSMUSG00000068129	66.028	1.634	0.010
Cd68	ENSMUSG00000018774	761.094	0.557	0.006
Nsg1	ENSMUSG00000029126	118453.175	-0.214	0.041
H2-Q7	ENSMUSG00000060550	461.700	0.761	0.001
Nsg2	ENSMUSG00000020297	17203.283	0.363	0.012
Ctsd	ENSMUSG00000007891	33856.962	0.382	< 0.001
2610002M06Rik	ENSMUSG00000031242	7455.780	-0.157	0.038
Prkcd	ENSMUSG00000021948	15130.466	-0.240	0.012
Rab38	ENSMUSG00000030559	74.954	1.387	0.042
Ctss	ENSMUSG00000038642	8398.508	0.350	< 0.001
Tmem25	ENSMUSG00000002032	16856.246	-0.150	0.035
Apoe	ENSMUSG00000002985	294918.992	0.315	0.003
Unc13d	ENSMUSG00000057948	1948.570	-0.298	0.025
Cst3	ENSMUSG00000027447	72853.485	0.250	0.046
Arl8a	ENSMUSG00000026426	23966.848	-0.112	0.040
Cd63	ENSMUSG00000025351	16922.196	0.306	0.003
H2-Q4	ENSMUSG00000035929	1712.362	0.637	< 0.001
H2-Q6	ENSMUSG00000073409	605.404	0.610	0.017
Slc11a1	ENSMUSG00000026177	351.078	0.472	0.006
Tinagl1	ENSMUSG00000028776	1872.544	0.444	0.013
Gaa	ENSMUSG00000025579	42288.649	0.148	0.046
Npc2	ENSMUSG00000021242	13576.144	0.252	0.005
Cpq	ENSMUSG00000039007	3671.835	0.301	0.043
Naga	ENSMUSG00000022453	5578.299	0.171	0.009
Man2b2	ENSMUSG00000029119	5625.125	0.227	0.008
Gfap	ENSMUSG00000020932	49633.449	0.670	< 0.001
Hexb	ENSMUSG00000021665	11580.391	0.325	0.001
Lipa	ENSMUSG00000024781	3011.385	0.339	0.003
Meak7	ENSMUSG00000034105	1681.762	0.255	0.012
Ifi30	ENSMUSG00000031838	755.863	0.547	< 0.001
Trip10	ENSMUSG00000019487	1776.641	0.312	0.029
Borcs8	ENSMUSG00000002345	2644.624	-0.392	< 0.001
Myo7a	ENSMUSG00000030761	5484.873	0.552	< 0.001
Syt7	ENSMUSG00000024743	66668.649	-0.232	0.001
Gusb	ENSMUSG00000025534	2558.973	0.185	0.017
Rnf19b	ENSMUSG00000028793	28209.761	-0.243	0.038
Ctsc	ENSMUSG00000030560	1554.587	0.610	0.003
Laptm5	ENSMUSG00000028581	2659.155	0.278	0.006
Acp5	ENSMUSG00000001348	57.183	1.434	0.004
Inpp5f	ENSMUSG00000042105	25096.641	-0.158	0.005

Rusc1	ENSMUSG00000041263	8435.506	-0.146	0.044
Pld1	ENSMUSG00000027695	1492.635	0.305	0.013
Ticam2	ENSMUSG00000056130	58.459	1.110	0.010
Rassf9	ENSMUSG00000044921	702.197	0.316	0.017
Mr1	ENSMUSG00000026471	1753.049	0.342	0.006
Ece1	ENSMUSG00000057530	21877.619	-0.213	0.007
Sh3gl3	ENSMUSG00000030638	1097.889	0.255	0.046
Ptprf	ENSMUSG00000033295	6447.473	0.311	0.032
Washc2	ENSMUSG00000024104	71355.731	-0.263	0.033
Syndig1	ENSMUSG00000074736	15931.471	-0.199	0.019
Pld4	ENSMUSG00000052160	865.562	0.329	0.046
Ackr4	ENSMUSG00000079355	668.906	0.813	< 0.001
Unc93b1	ENSMUSG00000036908	1732.922	0.268	0.014
Rab11a	ENSMUSG00000004771	12908.215	-0.146	0.028
Rnd2	ENSMUSG00000001313	14349.243	0.181	0.030
H2-Ab1	ENSMUSG00000073421	394.199	0.802	0.005
Pacsin1	ENSMUSG00000040276	65047.878	-0.166	0.017
Ackr3	ENSMUSG00000044337	1329.920	0.292	0.032
Snap25	ENSMUSG00000027273	334660.707	-0.225	0.005
Map2k1	ENSMUSG00000004936	25321.319	-0.117	0.046
Cd22	ENSMUSG00000030577	81.223	0.856	0.003
Nrp1	ENSMUSG00000025810	1247.448	0.283	0.042
Kcnj11	ENSMUSG00000096146	7056.627	-0.188	0.025
Fcgrt	ENSMUSG00000003420	4913.386	0.239	0.013
Dgkh	ENSMUSG00000034731	13465.118	-0.264	0.022
Bsg	ENSMUSG00000023175	98426.046	0.221	0.048
Rnf128	ENSMUSG00000031438	4114.551	-0.181	0.016
Stambpl1	ENSMUSG00000024776	2576.502	-0.196	0.023
Cpne6	ENSMUSG00000022212	2074.575	0.537	0.003
Ccr5	ENSMUSG00000079227	417.390	0.454	0.030
Dagla	ENSMUSG00000035735	19804.120	-0.336	0.012
Zfyve21	ENSMUSG00000021286	2110.324	0.191	0.021
Dner	ENSMUSG00000036766	118667.368	-0.372	< 0.001
Grb14	ENSMUSG00000026888	2737.028	0.223	0.030
Scoc	ENSMUSG00000063253	12593.242	-0.778	< 0.001
Mrc1	ENSMUSG00000026712	489.484	0.466	0.045
Epn3	ENSMUSG00000010080	4581.906	0.446	0.009
Gfra1	ENSMUSG00000025089	1244.452	0.557	0.006
Tpd52l1	ENSMUSG00000000296	1312.485	0.471	0.033
Vcam1	ENSMUSG00000027962	3713.941	0.429	< 0.001
Spns2	ENSMUSG00000040447	9562.590	-0.159	0.029

Table 2: List of antibodies

Antigen	Antibody (host)	Supplier	Catalog #	Dilution	Figure

EEA1	Anti-EEA1 monoclonal (mouse)	Sigma	E7659	1:500	2, 6, Supp. 4, 5
BDNF	Anti-BDNF monoclonal (rabbit)	Abcam	ab108319	1:500	2, 4, 6, Supp. 4
TrkB	Anti-TrkB polyclonal (rabbit)	EMD Millipore	ab9872	1:500	2, 3, Supp. 5
Stx13	Anti-Stx13 polyclonal (goat)	R & D systems	AF6617	1:500	3
Calbindin	Anti-calbindin polyclonal (guinea pig)	Synaptic Systems	214 004	1:500	2, 3, Supp. 4, 5
Rab7	Anti-Rab7 monoclonal (mouse)	Cell signaling technology	95746	1:400	4
Calbindin	Anti-calbindin monoclonal (mouse)	Swant	300	1:500	5
Lamp1	Anti-Lamp1 monoclonal (rat)	DSHB (University of Iowa)*	1D4B	1:400	5
Stx13	Anti-Stx13 polyclonal (rabbit)	Synaptic systems	110 133	1:150	Supp. 1
TrkB	Anti-TrkB polyclonal (rabbit)	Abcam	ab18987	1:500	Supp. 4
Anti-mouse secondary	Alexa 488 anti-mouse	Jackson Immunoresearch	AB_2338840	1:1000	2, 6, Supp. 4, 5
Anti-rabbit secondary	Alexa 594 anti-rabbit	Jackson Immunoresearch	AB_2340621	1:1000	2, 3, 6, Supp. 4, 5
Anti-mouse secondary	Alexa 594 anti-mouse	Jackson Immunoresearch	AB_2338871	1:1000	4
Anti-rabbit secondary	Alexa 488 anti-rabbit	Jackson Immunoresearch	AB_2313584	1:1000	4
Anti-rat secondary	Alexa 488 anti-rat	Invitrogen	AB_2313584	1:1000	5
Anti-goat secondary	Alexa 488 anti-goat	Jackson Immunoresearch	AB_2340428	1:1000	3
Anti-mouse secondary	DyLight 405 anti-mouse	Invitrogen	35501BID	1:500	5
Anti-guinea pig secondary	DyLight 405 anti-goat	Jackson Immunoresearch	AB_2340426	1:500	2, 3, Supp. 4, 5

*The LAMP-1 monoclonal antibody was obtained from the Developmental Studies Hybridoma Bank, created by the NICHD of the NIH and maintained at The University of Iowa, Department of Biology, Iowa City, IA 52242. It was deposited to the DSHB by August, J.T.

Acknowledgements

We would like to thank all members of the Watt lab for helpful discussions and feedback on experiments, particularly to Kim Gruver for feedback on an earlier draft of this manuscript. Thank you to Anne McKinney, Louis-Charles Masson and Andy Gao for advice and guidance throughout the project. Thank you to Rose Bagot for technical advice regarding the RNA-Sequencing experiment.

We are grateful to Lois Lau and Anika Holur for carrying out genotyping and to Tanya Koch and all CMARC staff for animal colony support. Imaging was carried out in the McGill University Advanced BioImaging Facility (ABIF), RRID:SCR_017697 and we thank ABIF staff members for technical support. This research was enabled in part by support provided by Calcul Québec (calculquebec.ca) and the Digital Research Alliance of Canada (alliancecan.ca).

This work was funded by a CIHR project grant (PJT-153150) (AJW). Student support came from doctoral awards from the Fonds de recherche du Québec – Santé (AAC and TCSL), a MITACS training award (AAC), a McGill science undergraduate research award (MR), and a McGill Biology research award (ÉZD).

References

Akizu N, Cantagrel V, Zaki MS, Al-Gazali L, Wang X, Rosti RO, Dikoglu E, Gelot AB, Rosti B, Vaux KK, Scott EM, Silhavy JL, Schroth J, Copeland B, Schaffer AE, Gordts PLSM, Esko JD, Buschman MD, Field SJ, Napolitano G, Abdel-Salam GM, Ozgul RK, Saglroglu MS, Azam M, Ismail S, Aglan M, Selim L, Mahmoud IG, Abdel-Hadi S, Badawy A El, Sadek AA, Mojahedi F, Kayserili H, Masri A, Bastaki L, Temtamy S, Müller U, Desguerre I, Casanova JL, Dursun A, Gunel M, Gabriel SB, De Lonlay P, Gleeson JG. 2015. Biallelic mutations in SNX14 cause a syndromic form of cerebellar atrophy and lysosome-autophagosome dysfunction. *Nat Genet 2015 475* **47**:528–534. doi:10.1038/ng.3256

Alves S, Cormier-Dequaire F, Marinello M, Marais T, Muriel MP, Beaumatin F, Charbonnier-Beaupel F, Tahiri K, Seilhean D, El Hachimi K, Ruberg M, Stevanin G, Barkats M, den Dunnen W, Priault M, Brice A, Durr A, Corvol JC, Sittler A. 2014. The autophagy/lysosome pathway is impaired in SCA7 patients and SCA7 knock-in mice. *Acta Neuropathol* **128**:705–722. doi:10.1007/s00401-014-1289-8

Anders S, Pyl PT, Huber W. 2015. HTSeq—a Python framework to work with high-throughput sequencing data. *Bioinformatics* **31**:166–169. doi:10.1093/BIOINFORMATICS/BTU638

Birgisdottir ÅB, Johansen T. 2020. Autophagy and endocytosis – interconnections and interdependencies. *J Cell Sci* **133**. doi:10.1242/JCS.228114/224826

Bonam SR, Wang F, Muller S. 2019. Lysosomes as a therapeutic target. *Nat Rev Drug Discov 2019 1812* **18**:923–948. doi:10.1038/s41573-019-0036-1

Bucci C, Bakke O, Progida C. 2012. Charcot–Marie–Tooth disease and intracellular traffic. *Prog Neurobiol* **99**:191. doi:10.1016/J.PNEUROBIO.2012.03.003

Cataldo AM, Barnett JL, Pieroni C, Nixon RA. 1997. Increased Neuronal Endocytosis and Protease Delivery to Early Endosomes in Sporadic Alzheimer's Disease: Neuropathologic Evidence for a Mechanism of Increased β-Amyloidogenesis. *J Neurosci* **17**:6142–6151. doi:10.1523/JNEUROSCI.17-16-06142.1997

Cataldo AM, Petanceska S, Terio NB, Peterhoff CM, Durham R, Mercken M, Mehta PD, Buxbaum J, Haroutunian V, Nixon RA. 2004. Aβ localization in abnormal endosomes: association with earliest Aβ elevations in AD and Down syndrome. *Neurobiol Aging* **25**:1263–1272. doi:10.1016/J.NEUROBIOLAGING.2004.02.027

Cataldo AM, Peterhoff CM, Troncoso JC, Gomez-Isla T, Hyman BT, Nixon RA. 2000. Endocytic pathway abnormalities precede amyloid β deposition in sporadic alzheimer's disease and down syndrome: Differential effects of APOE genotype and presenilin mutations. *Am J Pathol* **157**:277–286.

670 doi:10.1016/S0002-9440(10)64538-5
671 Chai Y, Koppenhafer SL, Shoesmith SJ, Perez MK, Paulson HL. 1999. Evidence for Proteasome
672 Involvement in Polyglutamine Disease: Localization to Nuclear Inclusions in SCA3/MJD and
673 Suppression of Polyglutamine Aggregation in vitro. *Hum Mol Genet* **8**:673–682.
674 doi:10.1093/HMG/8.4.673
675 Chang HHV, Cook AA, Watt AJ, Cullen KE. 2022. Loss of Flocculus Purkinje Cell Firing Precision Leads
676 to Impaired Gaze Stabilization in a Mouse Model of Spinocerebellar Ataxia Type 6 (SCA6). *Cells* **11**.
677 doi:10.3390/cells11172739
678 Chazotte B. 2011. Labeling lysosomes in live cells with lysotracker. *Cold Spring Harb Protoc*
679 **6**:pdb.prot5571. doi:10.1101/pdb.prot5571
680 Chen CS, Chen WNU, Zhou M, Arttamangkul S, Haugland RP. 2000. Probing the cathepsin D using a
681 BODIPY FL-pepstatin A: Applications in fluorescence polarization and microscopy. *J Biochem*
682 *Biophys Methods* **42**:137–151. doi:10.1016/S0165-022X(00)00048-8
683 Chen J, Chua KW, Chua CC, Yu H, Pei A, Chua BHL, Hamdy RC, Xu X, Liu CF. 2011. Antioxidant
684 activity of 7,8-dihydroxyflavone provides neuroprotection against glutamate-induced toxicity.
685 *Neurosci Lett* **499**:181–185. doi:10.1016/J.NEULET.2011.05.054
686 Cheng PL, Song AH, Wong YH, Wang S, Zhang X, Poo MM. 2011. Self-amplifying autocrine actions of
687 BDNF in axon development. *Proc Natl Acad Sci U S A* **108**:18430–18435.
688 Cheng XT, Xie YX, Zhou B, Huang N, Farfel-Becker T, Sheng ZH. 2018. Revisiting LAMP1 as a marker
689 for degradative autophagy-lysosomal organelles in the nervous system. *Autophagy*.
690 doi:10.1080/15548627.2018.1482147
691 Cook AA, Jayabal S, Sheng J, Fields E, Leung TCS, Quilez S, McNicholas E, Lau L, Huang S, Watt AJ.
692 2022. Activation of TrkB-Akt signaling rescues deficits in a mouse model of SCA6. *Sci Adv* **8**:3260.
693 doi:10.1126/sciadv.abh3260
694 Cortes CJ, La Spada AR. 2015. Autophagy in Polyglutamine Disease: Imposing Order on Disorder or
695 Contributing to the Chaos? *Mol Cell Neurosci* **66**:53. doi:10.1016/J.MCN.2015.03.010
696 de Duve C. 2005. The lysosome turns fifty. *Nat Cell Biol 2005 79* **7**:847–849. doi:10.1038/ncb0905-847
697 Du X, Wang J, Zhu H, Rinaldo L, Lamar K-M, Palmenberg AC, Hansel C, Gomez CM. 2013. Second
698 Cistron in CACNA1A Gene Encodes a Transcription Factor Mediating Cerebellar Development and
699 SCA6. *Cell* **154**:118–133. doi:10.1016/J.CELL.2013.05.059
700 Du X, Wei C, Hejazi Pastor DP, Rao ER, Li Y, Grasselli G, Godfrey J, Palmenberg AC, Andrade J, Hansel
701 C, Gomez CM. 2019. α1ACT Is Essential for Survival and Early Cerebellar Programming in a Critical
702 Neonatal Window. *Neuron*. doi:10.1016/J.NEURON.2019.02.036
703 Evans SF, Irmady K, Ostrow K, Kim T, Nykjaer A, Saftig P, Blobel C, Hempstead BL. 2011. Neuronal
704 Brain-derived Neurotrophic Factor Is Synthesized in Excess, with Levels Regulated by Sortilin-
705 mediated Trafficking and Lysosomal Degradation. *J Biol Chem* **286**:29556–29567.
706 doi:10.1074/JBC.M111.219675
707 Gao L, Tian M, Zhao HY, Xu QQ, Huang YM, Si QC, Tian Q, Wu QM, Hu XM, Sun LB, McClintock SM,
708 Zeng Y. 2016. TrkB activation by 7, 8-dihydroxyflavone increases synapse AMPA subunits and
709 ameliorates spatial memory deficits in a mouse model of Alzheimer's disease. *J Neurochem* **136**:620–
710 636. doi:10.1111/JNC.13432
711 Haapasalo A, Sipola I, Larsson K, Åkerman KEO, Stoilov P, Stamm S, Wong G, Castrén E. 2002.
712 Regulation of TRKB Surface Expression by Brain-derived Neurotrophic Factor and Truncated TRKB
713 Isoforms. *J Biol Chem* **277**:43160–43167. doi:10.1074/JBC.M205202200
714 Han X, Zhu S, Wang B, Chen L, Li R, Yao W, Qu Z. 2014. Antioxidant action of 7,8-dihydroxyflavone
715 protects PC12 cells against 6-hydroxydopamine-induced cytotoxicity. *Neurochem Int* **64**:18–23.
716 doi:10.1016/J.NEUINT.2013.10.018
717 Hu YB, Dammer EB, Ren RJ, Wang G. 2015. The endosomal-lysosomal system: From acidification and
718 cargo sorting to neurodegeneration. *Transl Neurodegener*. doi:10.1186/s40035-015-0041-1
719 Huotari J, Helenius A. 2011. Endosome maturation. *EMBO J*. doi:10.1038/emboj.2011.286
720 Jayabal S, Chang HHV, Cullen KE, Watt AJ. 2016. 4-aminopyridine reverses ataxia and cerebellar firing

721 deficiency in a mouse model of spinocerebellar ataxia type 6. *Sci Rep*. doi:10.1038/srep29489
722 Jayabal S, Ljungberg L, Erwes T, Cormier A, Quilez S, El Jaouhari S, Watt AJ. 2015. Rapid onset of motor
723 deficits in a mouse model of spinocerebellar ataxia type 6 precedes late cerebellar degeneration.
724 *eNeuro* **2**:ENEURO.0094-15.2015. doi:10.1523/ENEURO.0094-15.2015
725 Jin LW, Maezawa I, Vincent I, Bird T. 2004. Intracellular Accumulation of Amyloidogenic Fragments of
726 Amyloid-β Precursor Protein in Neurons with Niemann-Pick Type C Defects Is Associated with
727 Endosomal Abnormalities. *Am J Pathol* **164**:975–985. doi:10.1016/S0002-9440(10)63185-9
728 Johnson RA, Lam M, Punzo AM, Li H, Lin BR, Ye K, Mitchell GS, Chang Q. 2012. 7,8-Dihydroxyflavone
729 exhibits therapeutic efficacy in a mouse model of Rett syndrome. *J Appl Physiol* **112**:704–710.
730 doi:https://doi.org/10.1152/japplphysiol.01361.2011
731 Kaur G, Lakkaraju A. 2018. Early endosome morphology in health and diseaseAdvances in Experimental
732 Medicine and Biology. Springer New York LLC. pp. 335–343. doi:10.1007/978-3-319-75402-4_41
733 Kaur G, Tan LX, Rathnasamy G, Cunza N La, Germer CJ, Toops KA, Fernandes M, Blenkinsop TA,
734 Lakkaraju A. 2018. Aberrant early endosome biogenesis mediates complement activation in the retinal
735 pigment epithelium in models of macular degeneration. *Proc Natl Acad Sci U S A* **115**:9014–9019.
736 doi:10.1073/pnas.1805039115
737 Kim D, Paggi JM, Park C, Bennett C, Salzberg SL. 2019. Graph-based genome alignment and genotyping
738 with HISAT2 and HISAT-genotype. *Nat Biotechnol 2019 378* **37**:907–915. doi:10.1038/s41587-019-
739 0201-4
740 Kim S, Ochoa K, Melli SE, Yousufzai FAK, Barrera ZD, Williams AA, McIntyre G, Delgado E, Bolish
741 JN, Macleod CM, Boghos M, Lens HP, Ramos AG, Wilson VB, Maloney K, Padron ZM, Khan AH,
742 Blanco RE, Soto I. 2023. Disruptive lysosomal-metabolic signaling and neurodevelopmental deficits
743 that precede Purkinje cell loss in a mouse model of Niemann-Pick Type-C disease. *Sci Reports 2023*
744 *131* **13**:1–17. doi:10.1038/s41598-023-32971-0
745 Klionsky DJ. 2005. Autophagy. *Curr Biol* **15**:R282–R283. doi:10.1016/J.CUB.2005.04.013
746 Koppel I, Aid-Pavlidis T, Jaanson K, Sepp M, Pruunsild P, Palm K, Timmusk T. 2009. Tissue-specific and
747 neural activity-regulated expression of human BDNF gene in BAC transgenic mice. *BMC Neurosci*
748 **10**:68. doi:10.1186/1471-2202-10-68
749 Lawrence RE, Zoncu R. 2019. The lysosome as a cellular centre for signalling, metabolism and quality
750 control. *Nat Cell Biol 2019 212* **21**:133–142. doi:10.1038/s41556-018-0244-7
751 Liu C, Chan CB, Ye K. 2016. 7,8-dihydroxyflavone, a small molecular TrkB agonist, is useful for treating
752 various BDNF-implicated human disorders. *Transl Neurodegener* **5**:2. doi:10.1186/s40035-015-
753 0048-7
754 Liu X, Qi Q, Xiao G, Li J, Luo HR, Ye K. 2013. O-Methylated Metabolite of 7,8-Dihydroxyflavone
755 Activates TrkB Receptor and Displays Antidepressant Activity. *Pharmacology* **91**:185–200.
756 doi:10.1159/000346920
757 Love MI, Huber W, Anders S. 2014. Moderated estimation of fold change and dispersion for RNA-seq data
758 with DESeq2. *Genome Biol* **15**. doi:10.1186/S13059-014-0550-8
759 Ludwig T, Griffiths G, Hoflack B. 1991. Distribution of newly synthesized lysosomal enzymes in the
760 endocytic pathway of normal rat kidney cells. *J Cell Biol* **115**:1561–1572.
761 doi:10.1083/JCB.115.6.1561
762 Mahapatra KK, Panigrahi DP, Praharaj PP, Bhol CS, Patra S, Mishra SR, Behera BP, Bhutia SK. 2019.
763 Molecular interplay of autophagy and endocytosis in human health and diseases. *Biol Rev* **94**:1576–
764 1590. doi:10.1111/BRV.12515
765 Majzoub RN, Wonder E, Ewert KK, Kotamraju VR, Teesalu T, Safinya CR. 2016. Rab11 and Lysotracker
766 Markers Reveal Correlation between Endosomal Pathways and Transfection Efficiency of Surface-
767 Functionalized Cationic Liposome-DNA Nanoparticles. *J Phys Chem B* **120**:6439–6453.
768 doi:10.1021/acs.jpcb.6b04441
769 Mannan AU, Roussa E, Kraus C, Rickmann M, Maenner J, Nayernia K, Krieglstein K, Reis A, Engel W.
770 2004. Mutation in the gene encoding lysosomal acid phosphatase (Acp2) causes cerebellum and skin
771 malformation in mouse. *Neurogenetics* **5**:229–238. doi:10.1007/S10048-004-0197-9/FIGURES/6

772 Mellesmoen A, Sheeler C, Ferro A, Rainwater O, Cvetanovic M. 2019. Brain Derived Neurotrophic Factor
773 (BDNF) Delays Onset of Pathogenesis in Transgenic Mouse Model of Spinocerebellar Ataxia Type
774 1 (SCA1). *Front Cell Neurosci* **12**:509. doi:10.3389/fncel.2018.00509
775 Moya-Alvarado G, Gonzalez A, Stuardo N, Bronfman FC. 2018. Brain-derived neurotrophic factor (BDNF)
776 regulates Rab5-positive early endosomes in hippocampal neurons to induce dendritic branching. *Front*
777 *Cell Neurosci* **12**. doi:10.3389/fncel.2018.00493
778 Moya-Alvarado G, Tiburcio-Felix R, Ibáñez MR, Aguirre-Soto AA, Guerra M V., Wu C, Mobley WC,
779 Perlson E, Bronfman FC. 2023. BDNF/TrkB signaling endosomes in axons coordinate CREB/mTOR
780 activation and protein synthesis in the cell body to induce dendritic growth in cortical neurons. *Elife*
781 **12**. doi:10.7554/eLife.77455
782 O'Sullivan MJ, Lindsay AJ. 2020. The endosomal recycling pathway—at the crossroads of the cell. *Int J*
783 *Mol Sci*. doi:10.3390/ijms21176074
784 Park HY, Kim GY, Hyun JW, Hwang HJ, Kim ND, Kim BW, Choi YH. 2012. 7,8-Dihydroxyflavone
785 exhibits anti-inflammatory properties by downregulating the NF-κB and MAPK signaling pathways
786 in lipopolysaccharide-treated RAW264.7 cells. *Int J Mol Med* **29**:1146–1152.
787 doi:10.3892/IJMM.2012.935/HTML
788 Parrini M, Ghezzi D, Deidda G, Medrihan L, Castroflorio E, Alberti M, Baldelli P, Cancedda L,
789 Contestabile A. 2017. Aerobic exercise and a BDNF-mimetic therapy rescue learning and memory in
790 a mouse model of Down syndrome. *Sci Rep* **7**:16825. doi:10.1038/s41598-017-17201-8
791 Pescosolido MF, Ouyang Q, Liu JS, Morrow EM. 2021. Loss of Christianson Syndrome Na+/H+
792 Exchanger 6 (NHE6) Causes Abnormal Endosome Maturation and Trafficking Underlying Lysosome
793 Dysfunction in Neurons. *J Neurosci* **41**:9235–9256. doi:10.1523/JNEUROSCI.1244-20.2021
794 Prekeris R, Klumperman J, Chen YA, Scheller RH. 1998. Syntaxin 13 mediates cycling of plasma
795 membrane proteins via tubulovesicular recycling endosomes. *J Cell Biol* **143**:957–971.
796 doi:10.1083/jcb.143.4.957
797 Raudvere U, Kolberg L, Kuzmin I, Arak T, Adler P, Peterson H, Vilo J. 2019. g:Profiler: a web server for
798 functional enrichment analysis and conversions of gene lists (2019 update). *Nucleic Acids Res*
799 **47**:W191–W198. doi:10.1093/NAR/GKZ369
800 Rueden CT, Schindelin J, Hiner MC, DeZonia BE, Walter AE, Arena ET, Eliceiri KW. 2017. ImageJ2:
801 ImageJ for the next generation of scientific image data. *BMC Bioinformatics* **18**:529.
802 doi:10.1186/s12859-017-1934-z
803 Schindelin J, Arganda-Carreras I, Frise E, Kaynig V, Longair M, Pietzsch T, Preibisch S, Rueden C,
804 Saalfeld S, Schmid B, Tinevez JY, White DJ, Hartenstein V, Eliceiri K, Tomancak P, Cardona A.
805 2012. Fiji: An open-source platform for biological-image analysis. *Nat Methods*.
806 doi:10.1038/nmeth.2019
807 Scott-Solomon E, Kuruvilla R. 2018. Mechanisms of Neurotrophin Trafficking via Trk Receptors. *Mol Cell*
808 *Neurosci* **91**:25. doi:10.1016/J.MCN.2018.03.013
809 Skjeldal FM, Strunze S, Bergeland T, Walseng E, Gregers TF, Bakke O. 2012. The fusion of early
810 endosomes induces molecularmotor- driven tubule formation and fission. *J Cell Sci* **125**:1910–1919.
811 doi:10.1242/jcs.092569
812 Solodkin A, Gomez CM. 2012. Spinocerebellar ataxia type 6. *Handb Clin Neurol* **103**:461–473.
813 doi:10.1016/B978-0-444-51892-7.00029-2
814 Song JW, Misgeld T, Kang H, Knecht S, Lu J, Cao Y, Cotman SL, Bishop DL, Lichtman JW. 2008.
815 Lysosomal Activity Associated with Developmental Axon Pruning. *J Neurosci* **28**:8993.
816 doi:10.1523/JNEUROSCI.0720-08.2008
817 Stenmark H. 2009. Rab GTPases as coordinators of vesicle traffic. *Nat Rev Mol Cell Biol 2009 108* **10**:513–
818 525. doi:10.1038/nrm2728
819 Sterling FR, D'Amico J, Brumfield AM, Huegel KL, Vaughan PS, Morris K, Schwarz S, Joyce M V.,
820 Boggess B, Champion MM, Maciuba K, Allen P, Marasco E, Koch G, Gonzalez P, Hodges S, Leahy
821 S, Gerstbauer E, Hinchcliffe EH, Vaughan KT. 2023. StARD9 is a novel lysosomal kinesin required
822 for membrane tubulation, cholesterol transport and Purkinje cell survival. *J Cell Sci* **136**.

823 doi:10.1242/JCS.260662/VIDEO-10
824 Tate BA, Mathews PM. 2006. Targeting the role of the endosome in the pathophysiology of Alzheimer's
825 disease: a strategy for treatment. *Sci Aging Knowledge Environ* **2006**.
826 doi:10.1126/SAGEKE.2006.10.RE2/ASSET/EA0BA019-D870-4C63-AD9F-
827 D51957355788/ASSETS/GRAPHIC/102006RE2F1.JPEG
828 Unno T, Wakamori M, Koike M, Uchiyama Y, Ishikawa K, Kubota H, Yoshida T, Sasakawa H, Peters C,
829 Mizusawa H, Watase K. 2012. Development of Purkinje cell degeneration in a knockin mouse model
830 reveals lysosomal involvement in the pathogenesis of SCA6. *Proc Natl Acad Sci U S A* **109**:17693–
831 8. doi:10.1073/pnas.1212786109
832 Vanier MT. 2010. Niemann-Pick disease type C. *Orphanet J Rare Dis*. doi:10.1186/1750-1172-5-16
833 Vidyadhara DJ, Lee JE, Chandra SS. 2019. Role of the Endolysosomal System in Parkinson's disease. *J*
834 *Neurochem* **150**:487. doi:10.1111/JNC.14820
835 Vitelli R, Santillo M, Lattero D, Chiariello M, Bifulco M, Bruni CB, Bucci C. 1997. Role of the small
836 GTPase RAB7 in the late endocytic pathway. *J Biol Chem* **272**:4391–4397.
837 doi:10.1074/jbc.272.7.4391
838 Vivacqua G, Renzi A, Carpino G, Franchitto A, Gaudio E. 2014. Expression of brain derivated neurotrophic
839 factor and of its receptors: TrKB and p75NT in normal and bile duct ligated rat liver. *Ital J Anat*
840 *Embryol* **119**:111–129. doi:10.13128/IJAE-15138
841 Watase K, Barrett CF, Miyazaki T, Ishiguro T, Ishikawa K, Hu Y, Unno T, Sun Y, Kasai S, Watanabe M,
842 Gomez CM, Mizusawa H, Tsien RW, Zoghbi HY. 2008. Spinocerebellar ataxia type 6 knockin mice
843 develop a progressive neuronal dysfunction with age-dependent accumulation of mutant CaV2.1
844 channels. *Proc Natl Acad Sci U S A* **105**:11987–92. doi:10.1073/pnas.0804350105
845 Yamashita N, Kuruvilla R. 2016. Neurotrophin signaling endosomes: Biogenesis, regulation, and functions.
846 *Curr Opin Neurobiol*. doi:10.1016/j.conb.2016.06.004
847 Zaidi N, Maurer A, Nieke S, Kalbacher H. 2008. Cathepsin D: A cellular roadmap. *Biochem Biophys Res*
848 *Commun*. doi:10.1016/j.bbrc.2008.08.099
849 Zhang Z, Liu X, Schroeder JP, Chan CB, Song M, Yu SP, Weinshenker D, Ye K. 2013. 7,8-
850 Dihydroxyflavone Prevents Synaptic Loss and Memory Deficits in a Mouse Model of Alzheimer's
851 Disease. *Neuropsychopharmacol 2014 393* **39**:638–650. doi:10.1038/npp.2013.243
852 Zhu F, Miao Y, Cheng M, Ye X, Chen A, Zheng G, Tian X. 2022. The CACNA1A Mutant Disrupts
853 Lysosome Calcium Homeostasis in Cerebellar Neurons and the Resulting Endo-Lysosomal Fusion
854 Defect Can be Improved by Calcium Modulation. *Neurochem Res* **47**:249–263. doi:10.1007/s11064-
855 021-03438-3
856 Zhuchenko O, Bailey J, Bonnen P, Ashizawa T, Stockton DW, Amos C, Dobyns WB, Subramony SH,
857 Zoghbi HY, Lee CC. 1997. Autosomal dominant cerebellar ataxia (SCA6) associated with small
858 polyglutamine expansions in the alpha 1A-voltage-dependent calcium channel. *Nat Genet* **15**:62–9.
859 doi:10.1038/ng0197-62
860